AD-A172 868 NUMERICAL STUDY OF FLOW TURNING PHENOMENON(U) NAVAL RESEARCH LAB WASHINGTON DC J D BAUM 10 OCT 86 NRL-MR-5868 1/1

UNCLASSIFIED F/G 21/2 NL

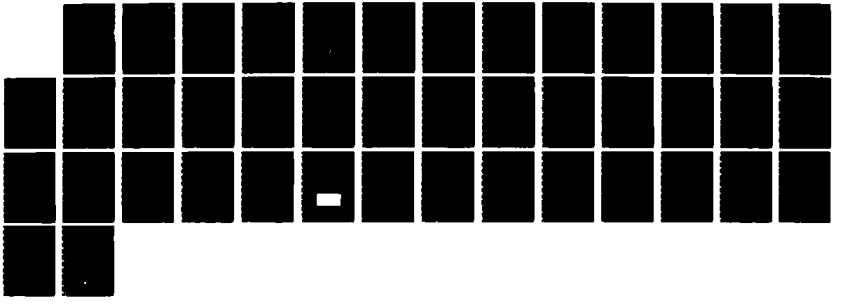

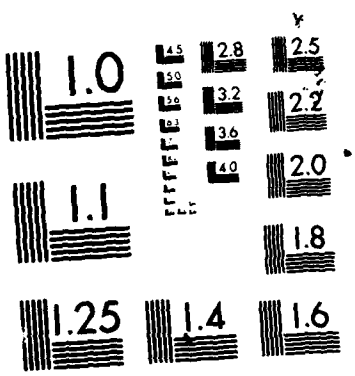

Numerical Study of Flow Turning Phenomenon

JOSEPH D. BAUM

Laboratory for Computational Physics

Approved for public release; distribution unlimited.

86 10 9 038

SECURITY CLASSIFICATION OF THIS PAGE

REPORT DOCUMENTATION PAGE

AD-A172868

1a REPORT SECURITY CLASSIFICATION UNCLASSIFIED	1b RESTRICTIVE MARKINGS
2a SECURITY CLASSIFICATION AUTHORITY	3 DISTRIBUTION/AVAILABILITY OF REPORT Approved for public release; distribution unlimited.
2b DECLASSIFICATION/DOWNGRADING SCHEDULE	
4 PERFORMING ORGANIZATION REPORT NUMBER(S) NRL Memorandum Report 5868	5 MONITORING ORGANIZATION REPORT NUMBER(S)
6a NAME OF PERFORMING ORGANIZATION Naval Research Laboratory	6b OFFICE SYMBOL (*If applicable*) Code 4040
6c ADDRESS (*City, State, and ZIP Code*) Washington, DC 20375-5000	7a NAME OF MONITORING ORGANIZATION 7b ADDRESS (*City, State, and ZIP Code*)
8a NAME OF FUNDING/SPONSORING ORGANIZATION Air Force	8b OFFICE SYMBOL (*If applicable*)
8c ADDRESS (*City, State, and ZIP Code*) Edwards AFB, CA 93523	9 PROCUREMENT INSTRUMENT IDENTIFICATION NUMBER 10 SOURCE OF FUNDING NUMBERS

PROGRAM ELEMENT NO	PROJECT NO	TASK NO	WORK UNIT ACCESSION NO
RDT&EAF			DN155-682

11 TITLE (*Include Security Classification*)
Numerical Study of Flow Turning Phenomenon

12 PERSONAL AUTHOR(S)
Baum, Joseph D.

13a TYPE OF REPORT	13b TIME COVERED	14 DATE OF REPORT (*Year, Month, Day*)	15 PAGE COUNT
Interim	FROM _____ TO _____	1986 October 10	42

16 SUPPLEMENTARY NOTATION

17 COSATI CODES			18 SUBJECT TERMS (*Continue on reverse if necessary and identify by block number*)
FIELD	GROUP	SUB-GROUP	

19 ABSTRACT (*Continue on reverse if necessary and identify by block number*)

The objective of the present research work is an understanding of the physical mechanisms by which energy is exchanged between the mean and acoustic flow fields in resonant combustion chambers (in particular, solid rocket motors). These processes may alter the balance between sources and sinks of oscillatory energy in the combustor significantly and thus are critical to our ability to predict the stability characteristics of proposed motor designs. The present report concentrates on the description and analysis of the computational results obtained to date in the study of acoustic refraction and flow turning phenomena.

Three studies were conducted. The time-dependent compressible Navier-Stokes equations were solved utilizing an implicit, non-iterative Linearized Block Implicit scheme. In the first study acoustic wave propagation in a tube with a coexisting sheared mean flow was investigated. The results demonstrate that acoustic refraction effects, i.e., the growth of acoustic pressure near the wall (for downstream propagation), are significant. In addition, the results demonstrate acoustic energy transfer to the mean flow as well as Richardson's

(Continues)

20 DISTRIBUTION/AVAILABILITY OF ABSTRACT	21 ABSTRACT SECURITY CLASSIFICATION
☒ UNCLASSIFIED/UNLIMITED ☐ SAME AS RPT. ☐ DTIC USERS	UNCLASSIFIED

22a NAME OF RESPONSIBLE INDIVIDUAL	22b TELEPHONE (*Include Area Code*)	22c OFFICE SYMBOL
Joseph D. Baum	(202) 767-3055	Code 4040

DD FORM 1473, 84 MAR 83 APR edition may be used until exhausted. All other editions are obsolete.

SECURITY CLASSIFICATION OF THIS PAGE

19. ABSTRACT (Continued)

annular effect. To the best of the authors' knowledge these are the first solutions demonstrating either Richardson's annular effect or refraction effects that are obtained through solution of the complete Navier-Stokes equations.

To help discriminate between acoustic energy loss due to artificial numerical dissipation and energy loss due to physical processes (including acoustic energy transfer to the mean flow) a second study was conducted in which acoustic wave propagation in a tube with no mean flow was investigated. The results, in agreement with experimental data, demonstrated that mean flow is excited by the acoustic flow field, a phenomenon referred to as acoustic streaming. Acoustic energy dissipation was significantly lower (per wave length) for this test case than for the acoustic refraction test case, indicating that although artificial energy dissipation due to numerical errors may not be completely eliminated, this energy loss is small in comparison to acoustic energy dissipation due to physical processes.

The third study investigated acoustic wave propagation in a tube with a coexisting mean flow, where the mean flow is injected into the tube through its lateral boundary. Results demonstrate the existence of Richardson's annular effect, the growth of the acoustic boundary layer due to wall blowing, the spatial growth of the pressure and axial velocity mean shifts (i.e. growth of energy contained in the mean flow field by energy transfer from the acoustic flow field), and the formation of a large new downstream directed axial velocity zone at the edge of the acoustic boundary layer, a phenomenon never reported before. Acoustic energy losses and mean pressure and axial velocity shifts were significantly higher for this test case than for the previous two tests due to the addition of flow turning losses. Though the present research was able to verify the existence of flow turning loss phenomenon, more theoretical and experimental research efforts are needed to help quantify flow turning loss and the several flow phenomena observed in this investigation.

CONTENTS

INTRODUCTION 1

Flow Turning 2

ACOUSTIC REFRACTION 6

Numerical Solution 7
Numerical Results 8

ACOUSTIC WAVE PROPAGATION WITH NO MEAN FLOW 13

Numerical Results 13

FLOW TURNING STUDY 15

Numerical Results 15
Root Mean Square and Time Averaged Calculations 18

ACOUSTIC ENERGY CALCULATIONS 20

CONCLUSIONS 21

ACKNOWLEDGMENTS 35

REFERENCES 35

NUMERICAL STUDY OF FLOW TURNING PHENOMENON

INTRODUCTION

The growth or decay of random small amplitude pressure oscillations in combustion systems is determined by a delicate balance between the driving and damping (i.e., sources and sinks) of oscillatory energy in the combustor. When the driving mechanisms outweigh the damping effects, small amplitude oscillations that are indigenous to the combustor chamber (i.e. random noise produced by the combustion or turbulence) can be amplified; a condition known as combustion instability. In solid or liquid propellant rocket motors, these sustained oscillations may affect guidance systems and alter the thrust time characteristics of the motor, or, in extreme cases, may result in significant overpressures and motor case failure.

The determination (both by theoretical predictions and experimental measurements) of the various acoustic energy sources and sinks in the combustion chamber is critical to our ability to predict *a priori* the stability characteristics of proposed solid propellant motor designs. The processes which dissipate acoustic energy include convection and radiation of acoustic energy through the nozzle (nozzle damping), the viscous and thermal losses produced by interaction of the condensed phase combustion products with the combustion gases (particle damping), the nonlinear viscoelastic characteristics of the grain and case (structural damping), viscous losses in the gas phase and at inert surfaces, gas phase vibrational relaxation effects, radiation of energy through the motor case and inelastic acceleration of combustion products leaving the propellant surface (flow turning). The primary source of oscillatory energy considered to date has been the response of the propellant combustion zone to acoustic pressure and acoustic velocity oscillations (termed pressure and velocity coupling, respectively). Other sources of energy include the combustion of incompletely reacted products in the chamber, distributed combustion of metal droplets in the gas phase, and conversion of mean flow energy to acoustic energy due to vortex shedding. The objective of the present research project is to seek an understanding of the physical mechanisms by which energy is exchanged between the mean and acoustic flow fields in resonant combustion chambers (in particular, solid rocket motors), processes

Manuscript approved July 15, 1986

that have been the subject of much speculation in the past, but which have never been thoroughly investigated. Specifically, the phenomena to be investigated are the interaction between the acoustic field in a chamber and a free shear layer (i.e., vortex shedding) and the so called "flow turning" effect.

FLOW TURNING

The term flow turning is commonly used to describe the loss of acoustic energy by the acoustic field in a combustor resulting from the inflow of combustion products through the lateral boundary of a combustion chamber containing longitudinal acoustic waves. The mean flow of solid propellant combustion products entering normal to the surface must turn to the axial direction parallel to the boundary in order to exit through the nozzle; simultaneously, each fluid element of the mean flow must acquire acoustic energy. It is this second process, involving the irreversible action of the unsteady field in the chamber upon the entering flow, which has been hypothesized to be a loss of energy for the existing acoustic field. This energy loss is often referred to as flow turning loss because mean flow turning is necessarily involved. However, it is really a rate of energy loss, proportional to the velocity of the incoming flow perpendicular to the boundary.

The modeling of flow turning involves multi-dimensional, rotational and viscous flow effects on widely varying distance scales. These effects only increase the difficulty of modeling this problem due to difficulties in both analytical and numerical procedures. Lack of a basic fundamental theory of mean flow-acoustic interactions has resulted in disagreement among researchers about a very basic point; namely, is flow turning a surface effect, a volume effect or a combination of the two? The experimental measurement of this acoustic energy loss mechanism is difficult since this effect usually appears in conjunction with other gain and loss mechanisms and cannot be easily isolated. The pioneering theoretical work of Culick[1,2] utilizing a one-dimensional, inviscid approximation is qualitative at best. The logic behind these approximations was challenged by several researchers working in the field [3,4]. Flandro's model[3] is locally two-dimensional and laminar. However, Flandro chose to neglect effects of rotational core flow and mean flow viscosity and to limit the model to small Mach numbers and small disturbance amplitudes. Chung's[5] formulation utilizes a three- dimensional, viscous analysis. The result of this analytical approach has not yet been compared to experiments. Culick[6] has qualitatively demonstrated the existence of this flow turning phenomenon, but due to the very low Mach number facility used to conduct the experiment, quantitative information could not be obtained.

Hersh[7] conducted an experimental investigation of the flow turning losses associated with the injection of steady lateral flow of cold air into a rectangular duct containing longitudinal acoustic waves. This experiment was designed to simulate injection of hot combustion products into a combustion chamber. The results indicated that the flow turning process absorbs sound (i.e., damping of acoustic energy). A one-dimensional model developed by Hersh[8] seriously underpredicted the measured acoustic energy losses. Hersh speculated that in addition to the flow turning absorption, there is another energy absorption mechanism related to acoustic refraction. Due to refraction by the mean flow velocity gradients, the sound pressure near the side wall increases, thereby enhancing the acoustic energy absorption by the finite admittance walls. Nevertheless, Hersh concluded that "most of the sound absorption appeared to take place within the fluid interior in support of Culick's ideas, but final interpretation of the data requires the development of a two-dimensional model of the flow turning process".

It is important to recognize that in addition to flow turning and refraction, several other physical mechanisms may have to be considered when an attempt is made to properly model acoustic-mean flow interactions. It had been demonstrated through analysis[9-12] and experiments[13-16] that the interaction between the mean and acoustic fields may (a) modify the turbulent structure of the flow; (b) accelerate transition to turbulence; (c) cause flow reversal during a portion of the wave cycle; and (d) inhibit or augment heat transfer to the boundaries. It has been demonstrated[17] that oscillating flows in a tube, even without mean flow, exhibit fully turbulent behaviour for Reynolds numbers higher than 3000. Richardson[9,18] measured the root mean square (termed here rms) velocity field in a circular tube in the absence of mean flow and identified the overshoot of the axial velocity at the edge of the acoustic boundary layer, a phenomenon now commonly referred to as Richardson's annular Effect. Mohajery[19] and Bogdanoff[14] observed, utilizing hot-wire measurements, that eddy viscosity increases significantly near the wall for acoustic wave propagation in the presence of mean flow at Reynolds numbers up to 10^5. More recently, Clamen[15] conducted a series of experiments using an hydrogen bubble technique to study water flow in a vibrating tube for low Reynolds numbers for a range of amplitudes and frequencies. Among the theoretical analyses, Sexl[20] obtained a solution for wave propagation in a tube with no mean flow, Uchida[10] extended his results to include laminar mean flow, and Romie[11] investigated harmonic wave propagation in laminar pipe flows for the study of heat transfer mechanism. More recently, Barnett[21] investigated the effect of longitudinal pressure oscillations on the velocity distribution in laminar and fully developed pipe flows. Barnett's analysis solved the incompressible, Reynolds-averaged, linearized Navier-Stokes equations. The solution was applied only to low Reynolds number flows. Barnett

demonstrated the existence of Richardson's annular effect and showed that: (a) acoustic boundary layer thickness is strongly influenced by mean flow Reynolds number and by the frequency of oscillations. For frequencies of interest in this research, but for significantly lower Reynolds numbers, the analysis predicted (based on a model developed by Richardson[22]) the acoustic boundary layer thickness to be within 0.0065 radii (for 1000 Hz) to 0.0026 radii (for 6000 Hz); (b) acoustic boundary layer thickness and maximum axial velocity overshoot vary during a cycle; and (c) the overshoot at the edge of the acoustic boundary layer varies directly with frequency.

To properly resolve energy transfer between the acoustic and mean flow field, it is necessary to utilize a numerical integration scheme that has very small diffusive and dispersive errors. In addition, the numerical scheme chosen has to handle very fine grid resolution near the wall in order to resolve energy transfer within the acoustic boundary layer, and a coarse grid resolution near the centerline. These grid variation requirements can be best satisfied by utilizing implicit integration schemes[23]. A drawback of the implicit codes is that they often utilize artificial viscosity to stabilize the solution. In addition, the truncation and splitting errors of the algorithms may act as artifical energy dissipation mechanisms. These numerically induced energy dissipation mechanisms can be minimized by reducing the artificial viscosity coefficient value used in the calculations and reducing the numerical integration time step. Nevertheless, these erroneous dissipation mechanisms cannot be eliminated entirely.

The primary objective of this research is to calculate the so called flow turning loss. This is done by calculating the axial and radial acoustic energy distributions for a downstream propagating wave as it traverses the length of a tube in which the mean flow is introduced into the tube through its perimeter. Before calculating acoustic energy it is necessary to distinguish between acoustical properties (properties that travel with the speed of sound) from properties that are convected by the flow. The separation of these properties in a flow that involves multi-dimensional rotational and viscous flow effects has never before been extensively studied or resolved. The most important question namely, the exact definition of acoustic energy in a rotational viscous flow, is left unanswered for the time being. Previous analytical work on this subject is currently beeing evaluated and its application to this specific problem will be made in the future. In the meantime, acoustic properties will be defined here as the difference between the time dependent and the steady properties. In order to get an approximate idea about acoustic energy losses in the system, the concept of acoustic energy that was derived for plane wave propagation in irrotational, inviscid flow (i.e. the time averaging of $p\dot{w}$) was adopted. This paper will concentrate on the description of the computational results obtained to date. Analysis of

the separation of the calculated properties and exact calculation of acoustic energy transfer will be the subject of future research.

The first case to be described is acoustic wave propagation in a tube with a coexisting sheared mean flow. Acoustic energy was expected to diminish due to both acoustic energy transfer to the mean flow, and through artificial energy dissipation due to the numerical errors of the integration scheme. To help quantify acoustic energy dissipation due to numerical errors, the calculations were repeated with significantly more mesh points both in the radial and axial directions simultaneously with a reduced integration time step. Acoustic wave propagation in a tube without mean flow will be described next. This test case was investigated to provide a baseline for evaluating the amount of erroneous numerical dissipation present in the solution. Though Richardson's annular effect and acoustic streaming had been observed for acoustic wave propagation with no mean flow[18], it was expected that for this test case, energy transfer between the acoustic and mean flows would be significantly reduced and most of the acoustic energy dissipated would result due to numerical errors.

The third test case to be described will be acoustic wave propagation in a tube with a coexisting sheared mean flow, where the mean flow was injected into the chamber through part of its lateral boundary. Comparison of axial and radial acoustic energy distributions for the three cases investigated should enable us the determination and quantification of the various acoustic energy dissipation mechanisms.

ACOUSTIC REFRACTION

When sound waves propagate in a moving medium (i.e., with a coexisting mean flow), the main physical processes affecting its propagation, in the absence of viscosity and thermal conduction, are convection and refraction. The sound is convected by the moving medium at its local velocity. In the presence of a sheared mean flow, local convection velocities are a function of position. This results in pressure gradients in the direction normal to the flow direction (i.e., in the radial direction, for the case of flow propagation in a hard-wall tube), which, in turn, results in the excitation of velocities normal to the flow. Thus, for the case of flow in a rigid tube, when the sound wave travels with the mean flow (downstream), the effect of velocity gradients is to refract the sound toward the wall. When the sound propagates against the mean flow (upstream) the effect of radial velocity gradient is to refract the sound toward the centerline. Schematics of downstream and upstream sound propagation are shown in Figs. 1a and 1b, respectively.

Previous research efforts to model and understand acoustic refraction phenomenon utilized linearized models[24–27]. For initially planar acoustic waves propagating downstream in a hard wall duct, the calculation indicated that the acoustic pressure at the wall is 100 db larger than at the centerline. This study also indicated that acoustic refraction effects increase with mean flow velocity and with the frequency of the oscillations. In succeeding studies[25–27] , the linearized treatment has been extended to treat sound propagation upstream in a long rigid tube as well as the effect of varying shear layer thickness. These studies indicated that for centerline Mach numbers in the range of 0.05 to 0.10 (flow velocities which are typical in solid motor chambers), the acoustic pressure amplitude near the propellant surface may be twice as large as the pressure amplitude at the centerline. Although nonlinear effects can be expected to significantly reduce the actual refractive enhancement of the near wall pressure, these results indicate that acoustic refraction, which has been virtually ignored in solid rocket stability analyses, may actually have quite important effects. This results from the fact that both the steady and transient response of the burning solid propellant are dependent upon the amplitude of the pressure and velocity oscillations near the burning surface.

An experiment to measure acoustic refraction effects is currently in progress[8,28]. In this experiment air is blown through a long rigid tube in which a plane wave is excited at the inlet. The mass flux through the tube was varied, resulting in a centerline Mach number variation from 0.038 to 0.10. The results, to date, indicate that the acoustic pressure is amplified near the pipe wall; the degree of amplification increases with Mach number.

With a centerline Mach number of 0.1 ($Re = 2.7 \times 10^5$) the measurements indicated a near wall acoustic pressure amplification of 40%. Such an increase in acoustic pressure amplitude may be critical for motor stability analysis. The discrepancy between the linear theory and the experimental data may possibly result from nonlinear mean flow-acoustic field interactions, which will tend to damp acoustic pressure growth near the walls. These processes are not modeled by the linear analysis.

NUMERICAL SOLUTION

Under the current research program, the MINT code was acquired and modified for the investigation of acoustic refraction and flow turning. The code solves the compressible Reynolds-averaged Navier-Stokes equations using an efficient, non-iterative time dependent Linearized Block Implicit (LBI) scheme.[29-30]. The current model utilizes either a turbulent kinetic energy-algebraic length scale ($\kappa - l$) model[31] or a transport turbulence ($\kappa - \epsilon$) model[32]. The later includes modifications[33] that allow the $\kappa - \epsilon$ model to be utilized throughout the entire viscous sublayer without any wall function assumptions. The resulting code was verified by comparing the predictions to experimental data[34] for flat plate boundary layer flows with and without wall transpiration. For a complete description of the equations solved and the turbulence models used see Reference 33.

The study of acoustic refraction utilizes a tube with a radius of 0.05 m (two inches) and a length of approximately five acoustic wavelengths (for any frequency studied). The temperature and the axial and radial components of the velocity are specified at the inlet plane, while constant static pressure was specified at the outflow plane. The calculation is initiated with a one-seventh power law velocity profile at the inlet plane, having a centerline Mach number of 0.1. After convergence to steady state, the pressure and axial velocities at the upstream boundary are perturbed continously to produce a system of downstream traveling waves in the computational domain. An exhaustive study of non-reflective boundary conditions demonstrated the inadequacy of all currently available models for low Mach number sheared flows. Thus, the solution was terminated when the front of the initial wave started reflecting from the downstream boundary.

Initial results for the refraction study were presented in Reference 23. These results were calculated on the Air Force Weapons Laboratory Cray 1-S computer. Many of these calculations were repeated on the Naval Research Laboratory Cray X-MP computer that has twice the online memory storage (core) and twice the speed of the Cray 1-S. The repeat calculations were conducted with approximately twice as many mesh points per wave length; a larger total number of points in the axial direction (currently about 250) which

in turn enabled integration over more wave cycles before the computation was terminated due to suspected wave reflection from the downstream boundary[23] (currently up to 6 wave cycles); more points in the radial direction (currently approximately 100) and a better distribution of mesh points next to the wall (the first mesh point a distance of only 4.2 μm away from the wall); and finally, to help overcome the first order accuracy of the MINT code, twice as many time steps per wave cycle are utilized (400 time steps compared to 200 previously). In addition, Scientific Research Associates of Hartford CT, graciously made available to the authors a partially vectorized version of the MINT code which is both faster (approximately 3.8 times faster) than the scalar code and due to improved code architecture, requires less storage for the identical grid size. The computational mesh for the flow refraction study utilizes 250 mesh points uniformly distributed in the axial direction and up to 100 points in the radial direction. Very fine mesh distribution is utilized near the wall, with an exponential growth of mesh spacing toward the centerline.

NUMERICAL RESULTS

The first test case utilized a frequency of 6000 Hz and centerline Mach number of 0.1. The time evolution of the radial distribution of acoustic pressure is shown in Fig. 2a. The initial plane wave is rapidly distorted as the wave propagates downstream. After 600 time steps, the amplitude of the acoustic pressure at the wall is 39.5% larger than at centerline. The corresponding time evolution of the radial distribution of the axial acoustic velocity is shown in Fig. 2b. The initial plane wave is distorted in time. After 600 time steps, the amplitude of axial velocity oscillations near the wall is 31% larger than at centerline. It should be pointed out that the amplitudes of both the acoustic pressure and the axial acoustic velocity were decreased as the wave propagated downstream.

These calculations were performed both on the Cray 1-S computer and the Cray X-MP computer. The calculations on the Cray X-MP computer were performed with a significant increase of mesh points per wave cycle and mesh points in the radial direction, combined with a significant decrease in the integration time step. Nevertheless, the repeat calculations resulted in pressure and axial acoustic velocity values (and thus, based on the definition of acoustic energy as $p\hat{w}$; acoustic energy) that were not significantly different (within a few percent) from the results obtained by utilizing the Cray 1-S computer. This observation does not imply that artificial numerical dissipation effects had been completely eliminated. Nevertheless, it suggests that numerical dissipation constitutes only an insignificant part of the total acoustic energy dissipated as the wave traverses the length of the computational domain.

Several other tests with different frequencies and centerline Mach numbers indicated that acoustic refraction effects: (a) increase with frequency; (b) increase with centerline Mach number; and (c) are higher for upstream wave propagation than for downstream wave propagation. In this connection it should be mentioned that linear theory results indicated the same trends. Nevertheless, the large refraction effects predicted by linear analysis are, as expected, significantly higher than those obtained via a solution of the Navier-Stokes equations.

Based on the classical solution for acoustic wave propagation in the presence of mean flow, the acoustic boundary layer thickness was calculated to be 330 μm for a frequency of 1000 Hz and 132 μm for 6000 Hz, for a fully developed pipe flow with centerline Mach number equal to 0.1. The additional (over previous calculations) number of mesh points distributed in the radial direction enabled better resolution of the acoustic boundary layer and better simulation of processes that describe transfer of information in the radial direction, especially inside the acoustic boundary layer. A wealth of information was obtained and several processes have been observed. Due to space and time limitations, only a few of these will be highlighted. Discussion of other results and further analysis of the results highlighted here will be deferred to future publications.

Figures 3 and 4 show the radial distribution of the acoustic pressure and axial velocity at an axial station located 1.32 m downstream from the left boundary, for the complete radius of the tube, and for an narrow zone near the wall, respectively. This test was conducted at a longitudinal frequency of oscillations of 1000 Hz. The radial distance is nondimensionalized by the radius (0 05 m), with the origin at the centerline. The results in Figs. 3a and 3b show typical radial distribution of acoustic pressure and axial acoustic velocity. These figures show the radial distribution of acoustic pressure and axial velocity at time equal 5.32 milliseconds (abbreviated henceforth to ms) and t= 5.72 ms, when the acoustic wave is near its maximum and minimum, respectively, at this location. Notice that the change of the acoustic pressure across the tube is relatively small at this time in the cycle. In this connection it should be mentioned that in a previous study[23] it was shown that the maximum variation of acoustic pressure across the tube cross-section for a downstream propagating wave at 1000 Hz was less than 1%. Figures 4a through 4f describe the transition of the acoustic pressure and axial acoustic velocity from the positive to the negative sign of waveform, where the positive waveform corresponds to a positive acoustic pressure and axial acoustic velocity (downstream directed) and a negative wave corresponds to negative acoustic pressure and axial acoustic velocity (upstream directed). At t=4.75 ms (shown in Fig. 4a) the acoustic wave just started decaying from its maximum value.

Notice the increase of acoustic pressure across the acoustic boundary layer (approximately 150 μm at this time) that results from acoustic refraction, and the overshoot of acoustic axial velocity at the edge of the acoustic boundary layer (Richardson's annular effect). Figure 4b shows that while the amplitudes of the acoustic pressure and axial velocities are decreasing, a further decrease is observed near the wall (within the acoustic boundary layer). This phenomenon is further enhanced at t=4.96 ms (Fig. 4c), at which time the axial acoustic velocity near the wall becomes negative. At t=5.03 ms (Fig. 4d) the acoustic pressure across the tube is still completely positive, while the axial acoustic velocity is positive everywhere, except near the wall. At this time the thickness of the newly formed acoustic boundary layer is only 68 μm. It should be noticed that simultaneously with the formation of a new acoustic boundary layer near the wall (with a negative velocity sign), the previous acoustic boundary layer (with a positive sign and its own overshoot) is propagating further into the core flow, with a thickness of approximately 500 μm (at t=5.02 ms). The acoustic pressure and axial acoustic velocity become negative only at t=5.05 ms, as shown in Fig. 4e. At a later time (5.25 ms, shown in Fig. 4f) the acoustic pressure profile across the acoustic boundary layer and across the tube diameter decrease in value, in accordance with refraction theory for upstream wave propagation.

The transition from a positive waveform to a negative waveform, shown in Figs. 4a through 4f, demonstrates that acoustic refraction effects result in increase of the absolute value of the acoustic pressure *with distance from the centerline*, independent of the sign of the wave. When the wave is positive, the acoustic pressure value near the wall is higher than the acoustic pressure value at centerline. When the wave is negative negative, the acoustic pressure value near the wall is, again, higher (in absolute value) than the acoustic pressure at centerline. Another phenomenon which is observed is the time variation of the acoustic boundary layer thickness. When the wave is near its maximum value (Fig. 4a), acoustic boundary layer thickness is approximately 150 μm. As the wave changes its sign, the acoustic boundary layer thickness starts growing from a zero value to 68 μm (Fig. 4d) and finally (Fig. 4f) reaches the same thickness as when the wave was at its maximum value (i.e., about 150 μm). Richardson's annular effect at the edge of the acoustic boundary layer, which is somewhat diminished in Figs. 3 due to scaling, is better observed in Figs. 4. In this connection it should be mentioned that the transition from a negative to a positive wave is of similar nature, i.e., the waveform transition occurs for the first time near the wall.

Another transition of interest is that of the radial acoustic velocity from a velocity directed away from the wall (negative sign) to a velocity directed toward the wall (positive sign). Before analyzing these results it should be mentioned that the analysis predicts

that the radial acoustic velocity leads the acoustic pressure and axial acoustic velocity by 90 degrees and that the maximum value of the radial acoustic velocity is approximately two orders of magnitude smaller than the maximum value of the axial acoustic velocity. The transition of the radial acoustic velocity is demonstrated utilizing results obtained for an acoustic wave propagation downstream (centerline Mach number equal to 0.1) at a frequency of 6000 Hz. Figures 5a through 5e show the radial distribution of the radial acoustic velocity for several times at a tube cross section located 0.158 m downstream from the left boundary. At t=0.5 ms the radial acoustic velocity has a minimum at approximately 0.60 radii. At later times the wave is distorted with the minimum approaching the wall while the positive component of the radial acoustic velocity starts growing near the centerline, at approximately 0.3 radii (as shown in Figs. 5b through 5c). During this time, the acoustic pressure and axial acoustic velocity are approaching their minima value, which they reach at t=0.56 ms. At this time the radial acoustic velocity is completely positive with an almost perfect symmetric distribution across the tube cross-section (Fig. 5f). The physical implication of the scenario depicted in this set of figures is that during the half wave cycle at which the acoustic pressure and axial acoustic velocity transition from a maximum value to their minimum value, the flow is pushed away from the wall towards the centerline (i.e. negative radial acoustic velocity). During the other half wave cycle, when the radial acoustic velocity is positive and the acoustic pressure and axial acoustic velocity transition from a minima values to their maxima values, the flow is pushed toward the wall. It is postulated here that acoustic refraction phenomenon is strongly influenced by the direction of the radial acoustic velocity. As the mass of the fluid is driven toward the wall by the positive radial acoustic velocity, the acoustic pressure at the wall becomes higher than the acoustic pressure at the centerline. When the flow is driven toward the centerline, the reverse occurs. Since radial velocity values are approximately two orders of magnitude lower than axial acoustic velocity values, the effect of refraction is small. In this connection it should be mentioned that for downstream wave propagation (for either 1000 Hz or 6000 Hz), it was found that the maximum value of the radial acoustic velocity is approximately twice as large as the minimum value.

To better correlate the results obtained with results available in the literature[18], results that are typically in the form of rms values, a computation of the acoustic values obtained at 1000 Hz were performed. A typical result is shown at an axial station located 0.515 m downstream of the left boundary. Figure 6 shows the near wall radial distribution of the acoustic pressure and the axial and radial components of the acoustic velocity. The axial acoustic velocity figure demonstrates Richardson's annular effect. The rms calculated value for the acoustic boundary layer thickness is approximately 180 μm, in good agreement

with approximate analysis predictions[20] and experimental trends[18]. In this connection it should be mentioned that, to the best of the authors knowledge these are the first solutions demonstrating either Richardson's annular effect or refraction effects that are obtained through solution of the complete Navier-Stokes equations.

As noted in the introduction, it was expected that the part of the acoustic energy of the waveform will be converted to mean flow energy. It was also expected that the planar wave introduced at the left boundary will exhibit an increasingly larger mean pressure and axial velocity shifts (indicating increase of the mean pressure and axial velocity values, respectively) as the wave propagated downstream. Only small mean pressure or axial velocity shifts is observed close to the left boundary. The phenomenon becomes more significant as the wave propagates downstream. Figures 7a through 7c show the time evolution of the acoustic pressure, axial acoustic velocity and acoustic energy for axial stations 35, 95, and 155 located on the centerline at distances of 0.291, 0.806 and 1.321 m, respectively, from the left boundary. It is shown that at station 35 (Fig. 7a) there is virtually no mean acoustic pressure or velocity shift and that the velocity and pressure are in phase. The situation changes as the wave propagates downstream. At station 95 (Fig. 7b) there is an observed mean pressure shift of approximtely 0.15% and a mean velocity shift of 0.1%. In addition, due to the mean pressure and axial velocity shifts, their minima are slightly out of phase, as observed in the acoustic energy information (i.e., negative acoustic energy). It should be noted that since the definition of acoustic energy was adopted from plane wave theory, negative acoustic energy simply implies that the acoustic pressure and axial acoustic velocity have opposite signs at a given instant of time, and cannot be interpreted as acoustic energy production or dissipation. At axial station 155 (Fig. 7c) the mean deviations are even larger. The mean pressure is shifted by approximately 0.25% and the mean axial velocity by 0.2%. The phase shift between these quantities is larger than before, as shown in the acoustic energy plot. While these numbers seem small they correspond to a significant percentage of the initial acoustic energy in the system. A disturbance with an initial pressure amplitude of 4.0% contains only 4.92% of the total energy. Thus, a mean pressure shift of 0.25% and a mean velocity shift of 0.2% represent a transfer of 9.1% of the initial acoustic energy to the mean flow energy. The increase in mean pressure remains approximately constant across the tube cross section at a given axial location. The mean axial velocity shift increases only slightly across most of the tube cross-section and starts changing considerably only within approximately 120 μm away from the wall, inside the acoustic boundary layer. Within this zone the axial velocity shift increases significantly and so does, consequently, the phase shift between the

axial acoustic velocity and the acoustic pressure. At a distance of 60 μm from the wall the mean velocity shift increase to 0.32% and at a distance of 17 μm from the wall, the mean velocity is shifted by approximately 0.57%. It is of interest to notice that inside the acoustic boundary layer the phase differences between the acoustic pressure and axial acoustic velocity increase toward the wall. At the wall, the axial acoustic velocity leads the acoustic pressure by approximately 30-40 degrees. The time evolution of acoustic pressure, axial acoustic velocity and acoustic energy at a point located 4.72 μm away from the wall is shown in Fig. 7d. While the time evolution of the acoustic pressure is almost identical to that observed at the centerline (Fig. 7c), with an identical mean pressure shift (0.25%), the axial acoustic velocity exhibits a nonlinear waveform with a mean shift of approximately 0.6%. These values imply that approximately 18% of the initial acoustic energy in the system had been converted to mean flow energy. The phase shift between the acoustic pressure and axial acoustic velocity is large enough to obtain negative acoustic energy values (i.e. the acoustic pressure and axial velocity have different signs) over a significant number of time steps.

ACOUSTIC WAVE PROPAGATION WITH NO MEAN FLOW

The computational mesh in the radial direction utilized for this test case was identical to the one used for the refraction test case. Since the objective was to integrate the solution for only three wave cycles (as opposed to 5 or 6 wavecycles in the refraction study), only 132 mesh points were used in the axial direction. The number of mesh points per wave cycle was held constant at 44. The longitudinal acoustic frequency was 1000 Hz.

NUMERICAL RESULTS

After propagating downstream for approximately three wavelengths, the amplitude of the acoustic pressure was reduced by about 12%, while the amplitude of the axial acoustic velocity was reduced by about 10%. This corresponds to roughly 8% acoustic energy reduction over three wavelengths.

As pointed out in the introduction, previous experimental[15,18] and theoretical[21] investigations demonstrated that when an acoustic wave propagates in a hard wall tube, with or without mean sheared flow, there is an excitation of a mean flow component at the edge of the acoustic boundary layer (i.e. Richardson's annular effect). The energy contained in the newly developed mean flow has to be taken out of the oscillatory field. This transfer of energy from the acoustic to the mean field by excitation of mean flow field velocity, often referred to as acoustic streaming, results in net energy gain to the mean flow in the

chamber (that may or may not exist there initially) and a net loss to the oscillatory field in the chamber.

Figures 8a through 8d show the radial distribution of the acoustic pressure, axial and radial acoustic velocities across the tube cross-section and expanded views near the wall at an axial station located a distance of 0.378 m downstream from the left boundary. Figures 8a and 8b show the radial variation at the time when the acoustic wave is near its minimum at this location (t=1.88 ms), while Figs.8c and 8d show the radial distribution half a wave cycle later, at t=2.31 ms. At this time the acoustic wave is near its maximum at this location. The radial distribution of acoustic pressure demonstrates small refraction effect. As mentioned previously, when sound waves propagate in a coexisting sheared mean flow, the effect of velocity gradients is to refract the sound. Since the solution was initiated with no mean flow, the small refraction effect observed indicates excitation of a sheared mean flow by the acoustic field. The steeper increase (in absolute value) of acoustic pressure inside the acoustic boundary layer is attributed to the larger axial acoustic velocity gradient at this location.

The acoustic boundary layer thickness is observed to vary in time during the cycle with a minimum value at the time the acoustic wave changes its sign and a maximum value at the time the acoustic wave is near its maximum or minimum value. Figures 9a through 9d show the radial variation of the axial acoustic velocity near the wall at four time instants during the transition of the wave from a negative waveform to a positive waveform. Figure 9a shows the radial distribution of the axial acoustic velocity at t=2.01 ms, just before the wave transitions from a negative to a positive waveform. The acoustic boundary layer thickness is 203 μm. Figure 9b (at t= 2.07 ms) shows that a new downstrem directed acoustic boundary layer has been formed near the wall, while the axial acoustic velocity everywhere else is still directed upstream (negative sign). Notice that the overshoot at the edge of the acoustic boundary layer is propagating toward the core flow as the acoustic boundary layer is growing. At t=2.09 ms (Fig. 9c) the downstream directed acoustic boundary layer continues to grow in value and expands deeper into the core flow, while the edge of the upstream directed boundary layer is now located 320 μm from the wall. Finally, at t=2.12 ms (Fig. 9d) the axial acoustic velocity across the complete tube is positive, with the large overshoot at the edge of the acoustic boundary layer, located a distance of 65 μm from the wall.

The rms calculated values at this axial location are shown in Fig. 10. The figure shows the acoustic boundary layer to have an average thicknesss of 250 μm, while Richardson[22] predicts a value of 330 μm. Since it is suspected that Richardson could not account for the

type of variation in acoustic boundary layer thickness depicted in Figs. 9a through 9d, it is postulated that the value of 330 μm is the maximum thickness of the acoustic boundary layer. This maximum value will yield an rms value of 233 μm, in good agreement with the computational predictions. In this connection it should be mentioned that the rms acoustic boundary layer thickness with no flow is thicker than acoustic boundary layer thickness with mean flow (250 μm vs 180 μm), in agreement with theoretical predictions[21] and experimental data[15] that show boundary layer thickness to decrease with increase of Reynolds number.

FLOW TURNING STUDY

The only test case conducted under this study was acoustic wave propagation downstream in a tube where the mean flow is injected into the tube through its lateral boundary (i.e. tube walls). The driven longitudinal acoustic frequency of oscillations was 1000 Hz. The geometry used for this test case is shown in Fig. 11. The length of the injection zone is 1.167 m, a distance that corresponds to approximately three wavelengths at a frequency of 1000 Hz. There are 137 points distributed uniformly in the axial direction along the blowing zone; yielding approximately 45 points per wave length. The injection Mach number is equal to 0.0021. After a steady state flow solution was obtained, the pressure and axial velocity at the upstream (left) boundary were perturbed sinusoidally to produce a system of downstream traveling waves in the computational domain.

NUMERICAL RESULTS

Figures 12a, 12b, 13a, and 13b show the radial distribution of acoustic pressure, axial acoustic velocity and radial acoustic velocity at two instants during a single wave cycle. Data are shown in the two figures for the complete radius and for an expanded view of the radial variation near the blowing wall. These results were obtained at an axial station located 1.004 m downstream from the left boundary and 0.163 m upstream from the end of the blowing zone. Figures 12a and 13a show the radial variation of the acoustic properties at t=4.24 ms. At this time the acoustic pressure and the axial acoustic velocity are about to reach their minima values while the radial acoustic velocity is about to transition from a velocity directed toward the centerline (negative sign) to a velocity directed toward the wall (positive sign). It is noted that for acoustic wave propagation downstream with wall blowing, the radial acoustic velocity leads the acoustic pressure by 90 degrees, as was observed for the previous two studies. The figures demonstrate that due to blowing from the wall, the acoustic boundary layer is significantly thicker than for acoustic wave propagation with or without mean flow. The acoustic boundary layer thickness varies between 260 to approximately 500 μm, as compared to rms values of 180 μm for the refraction test case

and 250 μm for the no mean flow case. The axial acoustic velocity overshoot at the edge of the acoustic boundary layer (Richardson's effect) is observed again. However, for the wall blowing test case this phenomenon is overshadowed by formation of an adjacent large positive (i.e., downstream directed) increase in the axial acoustic velocity. This positive increase has its maximum value at a distance of approximately 760 μm away from the injection wall. The axial acoustic velocity decays from this maximum overshoot value to its centerline value only at a distance of approximately 5000-6000 μm away from blowing surface. The value of the axial velocity at the maximum is 0.115 nondimensional units larger than the centerline value. In this connection it should be recalled that acoustic properties are defined here as the difference between the time dependent and the steady properties. Thus, they include, in addition to true acoustic properties, the temporal changes of the mean flow field.

Figures 12b and 13b show the radial distribution of acoustic pressure, axial, and radial acoustic velocities at t=4.67 ms; a difference of approximately half a wave cycle from the time for which the results presented in Figs. 12a and 13a were obtained. At this time the acoustic pressure and acoustic axial velocity are about to reach their maxima values while the radial acoustic velocity is about to change from a wall directed to a centerline directed (i.e. from a positive to a negative value). The variation of acoustic pressure across the acoustic boundary layer (due to refraction) is demonstrated in Fig. 13b. The overshoot of the axial acoustic velocity at the edge of the acoustic boundary layer is not immediately obvious in this figure, since the overshoot of the axial acoustic velocity and the larger value axial acoustic velocity positive overshoot that was also described previously, are now merged (since both are positive.) It is important to notice that the value of the axial acoustic velocity at the maximum of the "large positive overshoot" is again 0.115 nondimensional units higher than the value of the axial acoustic velocity at the centerline. An examination of several other radial distributions of the axial acoustic velocity at other times reveals that this large overshoot exists at any instant. Moreover, the maximum axial acoustic velocity value is consistently 0.115 nondimensional units higher than the value of the centerline axial acoustic velocity. In addition, although the centerline axial velocity changes signs every half wave cycle,this large scale axial velocity increase is always oriented downstream (i.e., in the plus direction). This indicates an addition to the mean axial velocity, and thus, an addition to the mean flow energy, in a zone extending from the edge of the acoustic boundary layer to a distance of approximately 5000-6000 μm away from the injection wall. The value and the location of the maximum value of this mean velocity shift (referred to henceforth as axial velocity mean, or dc, shift) varies with distance from the left boundary, as will be shown later. Nevertheless, it should be emphasized that at a

given location in the tube, the value of the axial velcoity dc shift is constant, independent of the value or the direction of the axial acoustic velocity at the centerline. To the best of the authors knowledge, this phenomenon has never been reported before.

The transition from a positive wave to a negative wave that was examined for the wave refraction study is significantly more complex for this case and involves information exchange between the radial acoustic velocity, pressure and axial acoustic velocity. A complete description of this transition would occupy several pages of discussion and figures and, due to lack of space, will be left for future papers. In this paper only the transition of axial acoustic velocity near the surface will be examined. Figures 14a through 14g show the radial distribution of the axial acoustic velocity near the blowing wall at several instants of time, at an axial station located 1.004 m from the left boundary. At t=4.19 ms (shown in Fig. 14a), when the axial acoustic velocity is near its minimum value, the thickness of the acoustic boundary layer is approximately 250 μm, and the overshoot of the axial acoustic velocity at the edge of the acoustic boundary layer is large. As the acoustic pressure and axial acoustic velocity values increase from their minima, transitioning to their maxima values, the overshoot is slightly diminished (as shown in Fig 14b). Figure 14c (at t=4.40 ms) shows that as the value of the centerline axial acoustic velocity is further increased (though still negative), the axial acoustic velocity near the wall becomes positive. An intriguing situation is further developed as a new acoustic boundary layer is developed inside the old acoustic boundary layer; the axial acoustic velocity at a zone near the wall is directed downstream while further away from the wall, inside the old acoustic boundary layer (with a thickness of 410 μm), as well as in the core flow, the velocity is still directed upstream (at time equal 4.43 ms and 4.45 ms, as shown in Figs 14d and 14e, respectively). The axial acoustic velocity is directed downstream across the complete tube only at t=4.51 ms. The downstream directed acoustic boundary layer thickness now starts growing with time. The overshoot at the edge of the acoustic boundary layer reaches a limiting value while the axial acoustic velocity everywhere else increases. Finally, as shown in Figs. 14f and 14g (for t=4.53 and t=4.61 ms, respectively), the large axial velocity dc shift merges with the overshoot at the edge of the acoustic boundary layer.

As stated earlier, this discussion is merely an indication of the complexity of the processes by which the acoustic signal changes its sign. For a full understanding of this process, the acoustic pressure and the axial and radial acoustic velocities need to be analyzed simultaneously at a region very near the wall as well as across the tube cross section. Nevertheless, even with the limited amount of information shown, it was clearly demonstrated that the transition is initiated at the blowing surface. The core flow transition occurs only after the transition inside the acoustic boundary layer had been completed.

ROOT MEAN SQUARE AND TIME AVERAGED CALCULATIONS

The root mean square calculations were expected to show the acoustic boundary layer thickness and Richardson's annular effect. The radial distribution of the root mean square (rms) calculated values of the acoustic pressure and axial and radial acoustic velocities are shown in Figs. 15a and 15b, for the complete radius and for an enlarged view of a zone near the wall, respectively, at a station located 0.377 m from the left boundary. The acoustic pressure data shows a small positive refraction effect across the tube diameter, a small undershoot at the edge of the acoustic boundary layer and an added acoustic pressure increase across the acoustic boundary layer. The rms axial acoustic velocity information demonstrates Richardson's annular effect with a significant overshoot at the edge of the acoustic boundary layer. The calculated rms thickness of the acoustic boundary layer is 330 μm. It is of interest to note that the radial acoustic velocity also has an increase at the edge of the acoustic boundary layer, unlike the rms calculated value for the mean flow claculations and similar to the results obtained for no mean flow. In this connection it should be mentioned that the radial acoustic velocity values for the wall blowing test case are significantly larger (at maximum or minimum) than the corresponding values obtained for the refraction test case, due to mean flow injection in the radial direction. In addition, it is noted that the maxima values of the radial acoustic wave were approximately twice as large as the minima values, as was observed for the flow with no wall injection.

Since mass is injected into the computational domain only through the forward part of the tube, downstream of the blowing zone the flow reverts slowly to the same flow pattern observed for acoustic wave propagation in the presence of mean flow but no wall blowing (i.e. the refraction test case). Figure 15c shows the radial distribution of acoustic pressure and axial and radial acoustic velocities near the hard wall at a station located 0.112 m downstream from the end of the blowing zone (1.279 m from the left boundary). The acoustic boundary layer shrank to approximately half the thickness predicted for the blowing zone (rms vlue of 190 μm vs. 330 μm in the blowing zone), and the undershoots and overshoots of acoustic pressure and radial acoustic velocity, respectively, at the edge of the acoustic boundary layer that were observed near the blowing zone, had now disappeared.

A potentially significant new phenomenon that was observed during the analysis of the transient results, namely, the axial velocity dc shift that started at the edge of the acoustic boundary layer, was not evident in the rms calculations. It is a dc phenomenon and as such cannot be evident in rms calculations. However, this type of phenomenon should be evident in time averaged calculations. Figures 16a through 16f, show the radial distribution of the axial acoustic velocity at six axial locations; stations 31, 51, 71, 91, 111 and 131 are located at distances of 0.257 m, 0.429 m, 0.600 m, 0.772 m, 0.944 m and 1.115 m

from the left boundary, respectively. All stations are located within the blowing zone. The mean axial velocity shift maximum is initially located at a distance of approximately 2250 μm away from the blowing wall (Fig. 16a). As the acoustic wave (initiated at the left boundary) propagates downstream over the blowing zone, the location of the time averaged mean velocity shift maximum is approaching the wall. At axial location 131 (Fig. 16f), the maximum is located approximately 660 μm away from the wall. In addition, as the acoustic wave propagates downstream along the blowing zone, the maximum value of the axial velocity dc shift increases. At station 31 this maximum value is 0.006 nondimensional units higher than the centerline time averaged acoustic axial velocity (Fig. 16a), 0.015 at station 51 (Fig. 16b) 0.026 at station 71 (Fig. 16c), 0.035 at station 91 (Fig. 16d), 0.042 at station 111 (Fig. 16e) and 0.048 at station 131 (Fig. 16f). In addition to this important increase in the maximum value of the axial velocity dc shift, these figures also demonstrate another very important fact; namely, the time averaged axial acoustic velocity at most points has a positive value. This implies that acoustic energy had been converted to mean flow energy even at the centerline; again demonstrating acoustic streaming effects.

The results obtained for the wave refraction study demonstrated mean pressure and axial velocity shifts, indicating transfer of energy from the acoustic field to the mean flow field. A similar investigation was conducted for the acoustic wave propagation in the presence of wall injection by analyzing both the spatial and temporal evolution of the acoustic waveform in the chamber. Figures 17a through 17c show the spatial evolution of acoustic pressure, axial acoustic velocity and acoustic energy, at t=4.20 ms, as a function of axial distance from the left boundary, for radial surfaces located on the centerline, 735 μm and 118 μm away from the wall, respectively. The spatial decay of both acoustic pressure and axial acoustic velocity as well as the growth of the mean pressure and axial velocity shifts are shown at all radial surfaces. It should be noticed that the disturbances observed in the axial acoustic velocity spatial evolution figures for radial surfaces near the wall (Fig. 17b and 17c) result due to the adjustment of the flow near the wall from a flow over a blowing wall to a flow over a hard wall (the blowing zone ends 1.16 m downstream of the left boundary). The continuous growth of the axial acoustic velocity (shown in Fig. 17b) is another demonstration of the continuous spatial growth of the axial velocity dc shift discussed in the previous paragraph, since this radial surface is located within the axial velocity dc shift zone.

Analysis of the time evolution of the acoustic pressure and axial acoustic velocity at several mesh points demonstrates that: (a) the mean pressure shift increases with distance from the left boundary and is approximately constant across the tube cross section (at

any given axial location); (b) the mean shift of axial velocity increases both in the axial and radial directions; and (c) the dc shifts of both pressure and axial acoustic velocity result in the growth of the negative component of the acoustic energy (i.e., the number of time instants in which the acoustic pressure and axial velocity have opposite signs) both in the axial and radial directions. Figures 18a through 18c show the time evolution of axial acoustic velocity at a tube cross-section located 1.059 m downstream from the left boundary; the three stations are located at the centerline, 624 μm from the blowing surface (close to the maximum of the axial velocity dc shift) and 96 μm from the blowing surface (within the acoustic boundary layer). The mean pressure shift at this axial location is approximately 0.23%. The mean axial velocity shift is only 0.1% at the centerline and grows toward the wall. Figure 18b shows that the shift in axial acoustic velocity still grows after one wave cycle. Based on experience gained in analyzing results obtained at points at the same radius but closer to the left boundary, points that experienced 4 or 5 wave cycles, it was concluded that the axial velocity mean shift stops growing after approximately two wave cycles. After two wave cycles the mean axial velocity shift at this location is approximately 0.9%. These values of mean pressure and axial velocity shifts imply that at this location approximately 23 percent of the initial acoustic energy had been converted to mean flow energy. Inside the boundary layer (Fig. 18c) the mean axial velocity shift is approximately 0.5%, while the waveform is nonlinear.

ACOUSTIC ENERGY CALCULATIONS

Figure 19 shows the comparison of normalized time averaged acoustic energy as a function of axial distance from the left boundary for three calculations: namely: acoustic wave propagaton with no mean flow, acoustic wave propagation in the presence of mean flow (acoustic refraction study) and acoustic wave propagation in a tube in which the mean flow is injected through the walls of the tube (flow turning study). All calculations were performed for an acoustic wave frequency of 1000 Hz. The time averaging calculations were performed for a distance of only one wavelength for the no-mean-flow results and for three wavelengths (the length of the blowing zone) for both the refraction and wall blowing test cases.

The figure shows that as the wave propagates downstream, reduction of acoustic energy is higher with mean sheared flow than with no mean flow and even higher with wall injection. Acoustic energy is reduced in the no mean flow case due to both artificial numerical dissipation and transfer of acoustic energy to the mean flow, as was shown during the discussion of the results. Since the exact definition of acoustic energy for

viscous, rotational flows has not been formulated yet, attempts to quantify acoustic energy transfer to the mean flow, and, by subtracting these losses from the total acoustic energy loss evaluate the numerical errors, will be left for future analysis. Nevertheless, it is shown that losses for the no-mean-flow test are significantly lower than losses for either the refraction or wall injection test cases. Higher acoustic energy losses for the refraction test case may indicate that: (a) more acoustic energy had been converted to mean flow energy, as observed in the analysis of the time dependent results; and (b) acoustic energy dissipation may increase due to the mean sheared flow. Finally, the figure shows that when the mean flow is injected through the wall, acoustic energy losses increase. As was noted previously, significantly larger mean pressure and axial velocity shifts were observed throughout the computational domain for the flow turning test case than for the refraction test case. . In addition, an even larger mean flow enhancement was observed at the edge of the acoustic boundary layer. Presently it is not immediately apparent how to quantify acoustic energy conversion to mean flow energy in a viscous, rotational field. Nevertheless, it is demonstrated that wall injection resulted in a significantly larger acoustic energy loss, part of which was converted to mean flow energy while the rest was dissipated.

CONCLUSIONS

This paper reports initial results obtained in a numerical investigation of acoustic energy exchange between the mean and acoustic flow fields through acoustic refraction, flow turning and acoustic streaming. The time- dependent compressible Navier-Stokes equations were solved utilizing an implicit, non-iterative Linearized Block Implicit scheme. Three test cases were investigated: acoustic propagation in a tube with a coexisting sheared mean flow (referred to as a refraction study), acoustic propagation in a tube with no mean flow, and acoustic propagation in a tube where the coexisting mean flow is injected into the tube through part of its lateral boundary (referred to as flow turning study).

The results of the refraction study demonstrated the effect of acoustic refraction. Several test cases were repeated on a more powerful computer (Cray X-MP) with reduced spatial and temporal errors. The results indicated that acoustic refraction effects: (a) increase with frequency; (b) increase with Mach number; (c) are higher for upstream wave propagation than for downstream wave propagation; and (d) are significantly lower than predicted by linear theory. Since acoustic refraction effects have the potential to enhance both páınd wńear the propellant and since the propellant transient burn rate is strongly dependent on these flow variables (through pressure and velocity coupling effects), it appears that acoustic refraction effects should be included in solid motor stability analyses.

The results obtained in all the three studies demonstrated Richardson's annular effect. The magnitude of the overshoot at the edge of the acoustic boundary layer and the boundary layer thickness changed in time during the wave cycle and changed from one test case to another. The acoustic boundary layer thickness was largest for the wall blowing case, as should be expected. The boundary layer thickness was larger for the no-mean-flow case than for the refraction test case since acoustic boundary layer thickness decreases with increase in Reynolds number.

All three cases demonstrated acoustic streaming effects. The largest mean pressure and axial velocity shifts were obtained for the flow turning case. The mean pressure shift increased with downstream propagation along the tube and was approximately constant at any axial cross-section. The mean axial velocity shift also increased with distance from the left boundary. In addition, the axial velocity shift increased significantly within the acoustic boundary layer. For the flow turning test case, an even larger mean axial velocity dc shift was observed within a zone adjacent to the acoustic boundary layer, extending a distance of up to 0.1 radii away from the wall. The distance between the wall and the location of the maximum value of this mean axial velocity shift was reduced with increase of distance from the left boundary while, simultaneously, the maximum value increased in value. Based on initial calculations it appears likely that a significant amount of acoustic energy is converted to mean flow field energy within this zone.

Complex flow phenomena occur as the acoustic field at a given location transitions from positive acoustic pressure and axial acoustic velocity to negative values, or from a radial acoustic velocity directed toward the wall (positive) to a radial velocity directed toward the centerline (negative velocity). It was shown that the radial acoustic velocity leads the acoustic pressure and axial acoustic velocity by 90 degrees and that near the wall, the axial acoustic velocity leads the acoustic pressure by approximately 30 degrees.

The results demonstrated that acoustic energy is diminished with distance from the inflow boundary. For acoustic wave propagation with no mean flow, this acoustic energy decrease results from to both acoustic energy transfer to the mean flow and artificial energy dissipation due to numerical errors. Acoustic energy losses increased significantly when sheared mean flow was introduced, as acoustic dissipation increased due to wave propagation in a viscous,rotational flow field. Finally, when the mean flow was injected into the tube through the lateral boundary, flow turning effects resulted in a significant increase of acoustic energy losses. Though the present research verified the existence of flow turning loss phenomenon, more theoretical and experimental efforts are needed to help quantify flow turning loss and the several flow phenomena observed in this investigation.

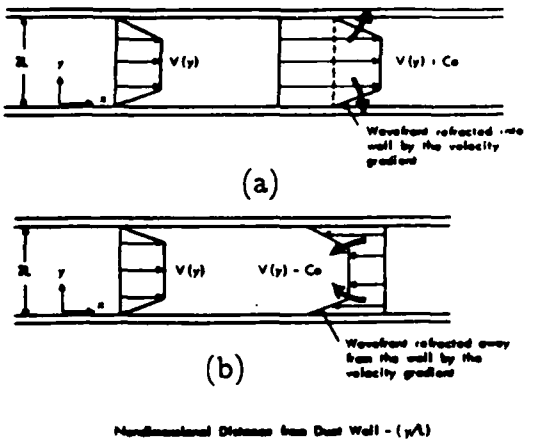

Fig. 1. (a) Schematic of Downstream Sound Propagation; (b) Schematic of Upstream Sound Propagation.

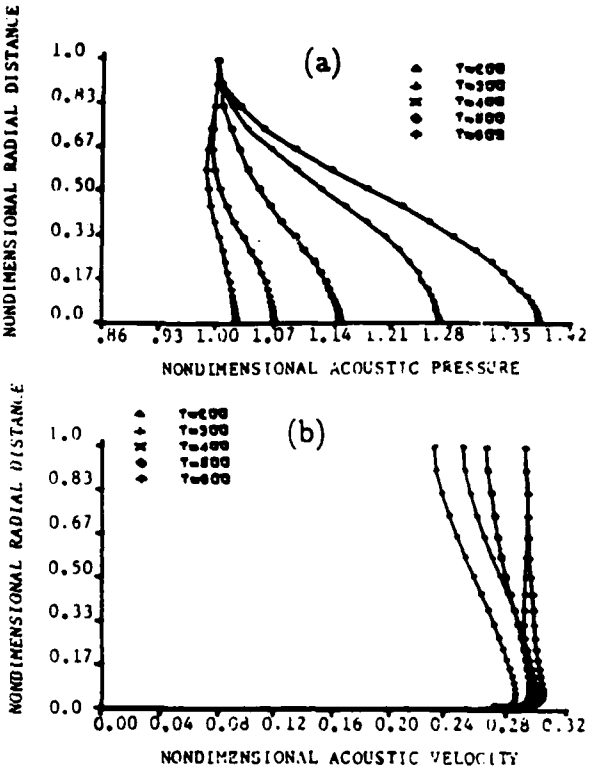

Fig. 2. Time Evolution of The Radial Distribution of: (a) Acoustic Pressure; (b) Axial Acoustic Velocity, f=6000 Hz, Mc.l.=0.1, Downstream Propagation.

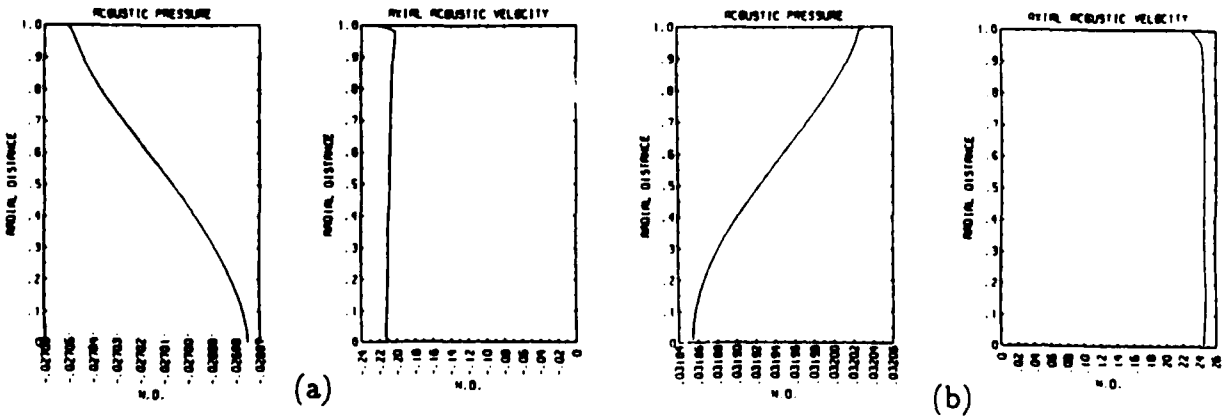

Fig. 3. Radial Distribution of Acoustic Pressure and Axial Acoustic Velocity, f=1000 Hz, Z=1.32 m. (a) Time=5.32 ms. (b) Time=5.77 ms.

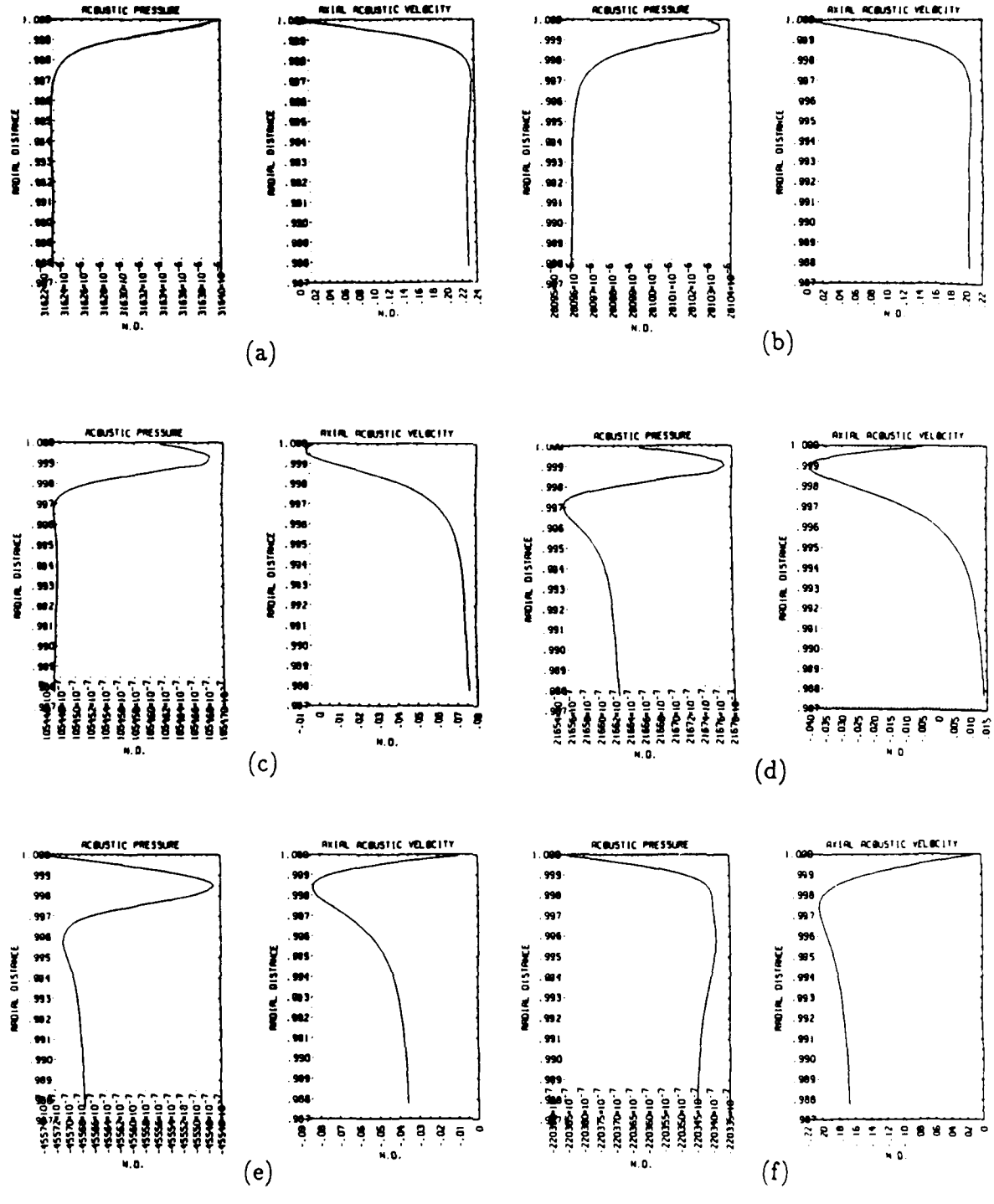

Fig. 4. Radial Distribution of Acoustic Pressure and Axial Acoustic Velocity Near The Wall, f=1000 Hz, Z=1.32 m. (a) Time=4.75 ms. (b) Time=4.80 ms. (c) Time=4.96 ms. (d) Time=5.03 ms. (e) Time=5.08 ms. (f) Time=5.24 ms.

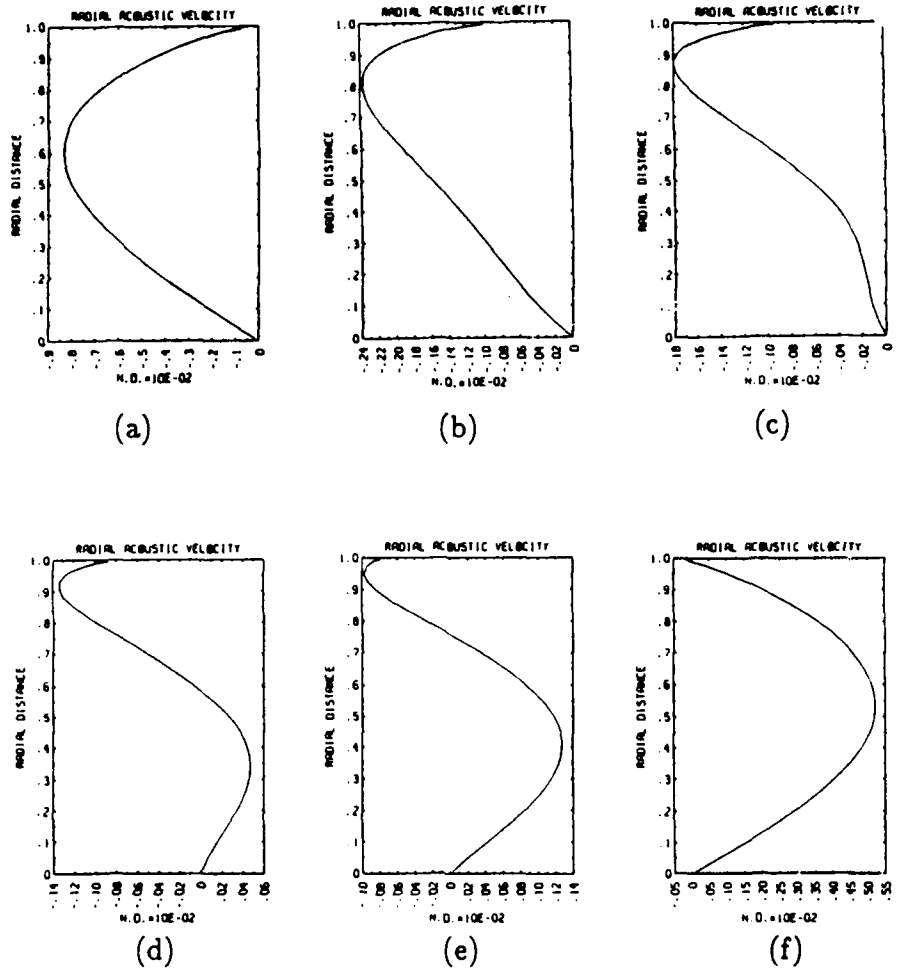

Fig. 5. Radial Distribution of Radial Acoustic Velocity, f=6000 Hz, Z=0.158 m. (a) Time=0.50 ms. (b) Time= 0.53 ms. (c) Time=0.542 ms. (d) Time=0.546 ms. (e)Time= 0.55 ms. (f) Time=0.56 ms.

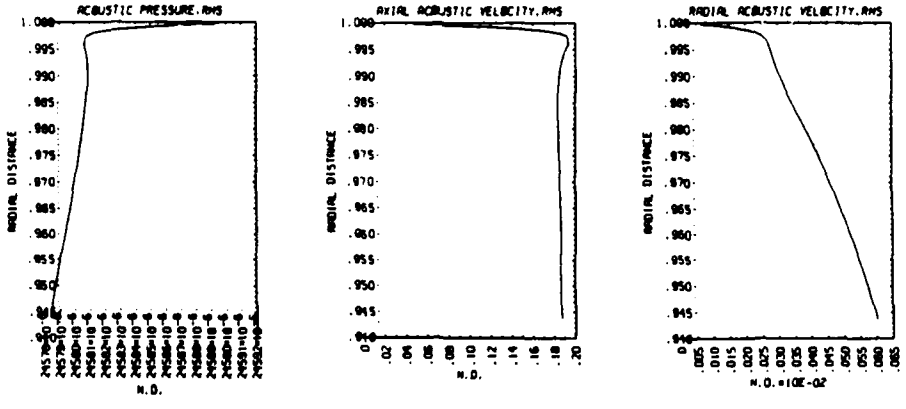

Fig. 6. Radial Distribution of Root-Mean-Squared Acoustic Pressure, Axial Acoustic Velocity and Radial Acoustic Velocity, f=1000 Hz, Z=0.515 m.

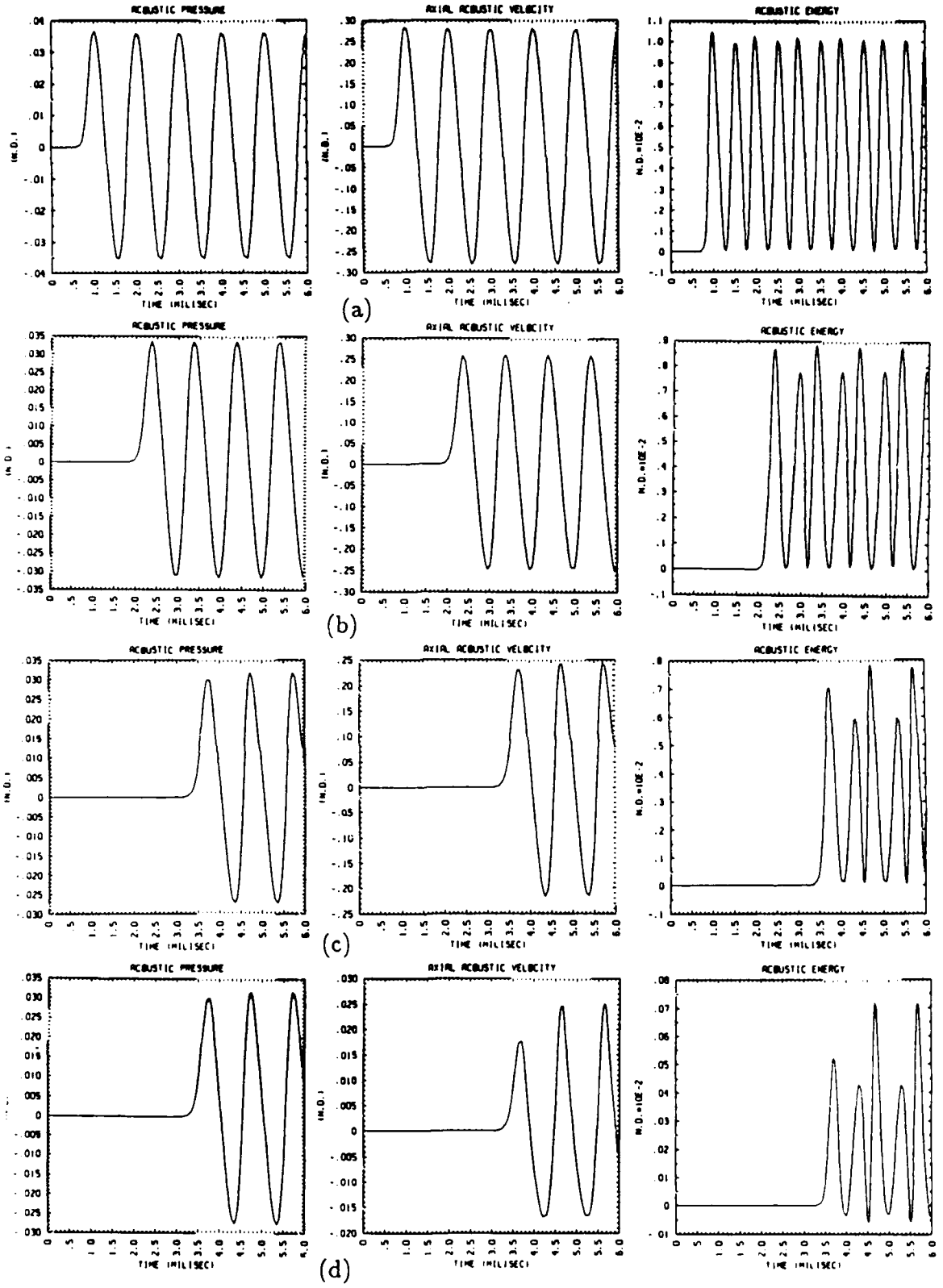

Fig. 7. Time Evolution of Acoustic Pressure, Axial acoustic Velocity and Acoustic Energy, f=1000 Hz. (a) Z= 0.291 m. Centerline. (b) Z=0.806 m. Centerline. (c) Z=1.321 m. Centerline. (d) Z=1.321 m. Distance to Wall=4.72 microns.

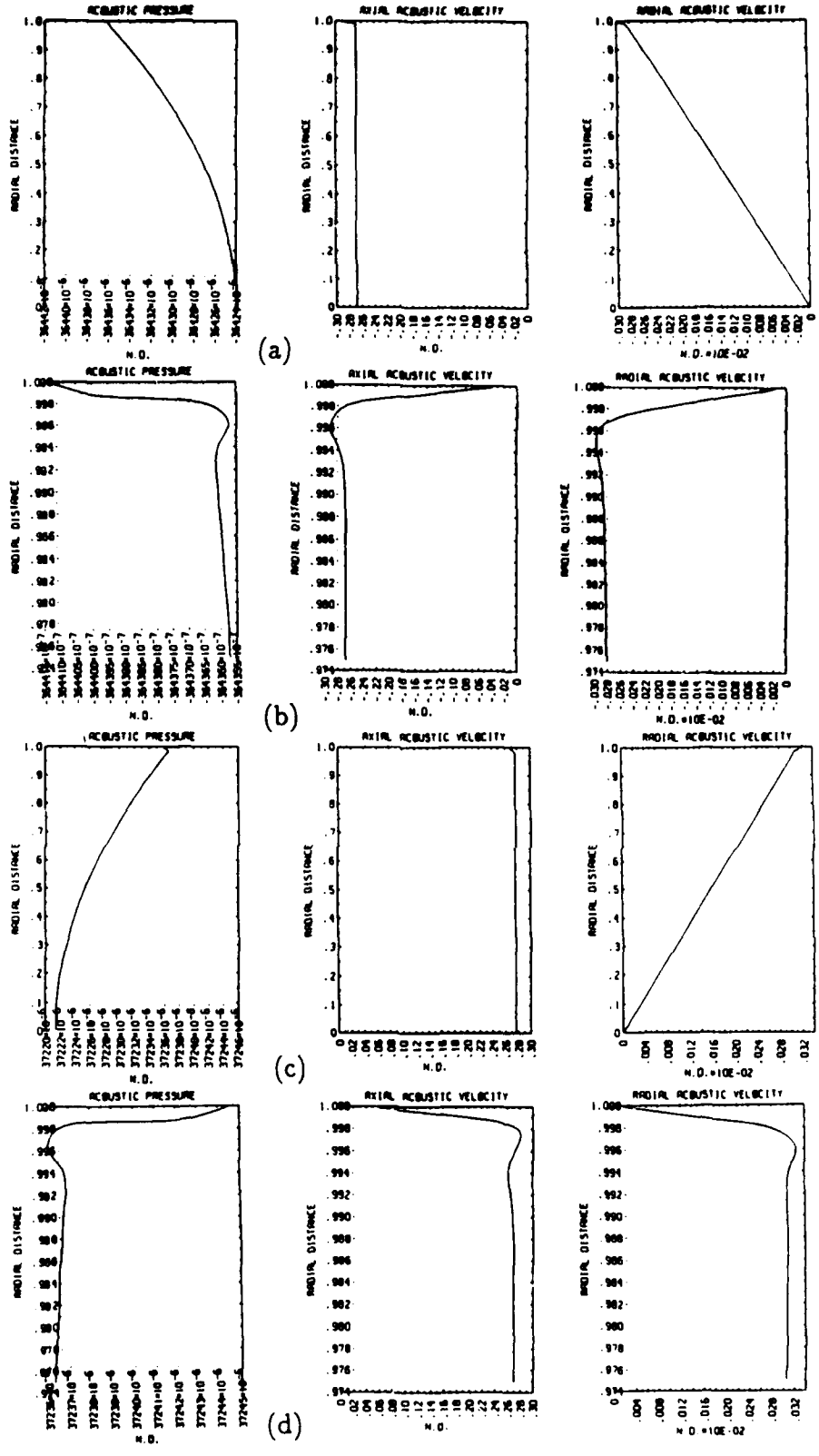

Fig. 8. Radial Distribution of Acoustic Pressure, Axial Acoustic Velocity and Radial Acoustic Velocity, No Mean Flow, f=1000 Hz, Z=0 378 m. (a) Time=1.88 ms. R=0.0-1.0. (b) Time=1.88 ms. R=0.978-1.0. (c) Time=2.31 ms. R=0.0-1.0. (d) Time=2.31 ms. R=0.978-1.0.

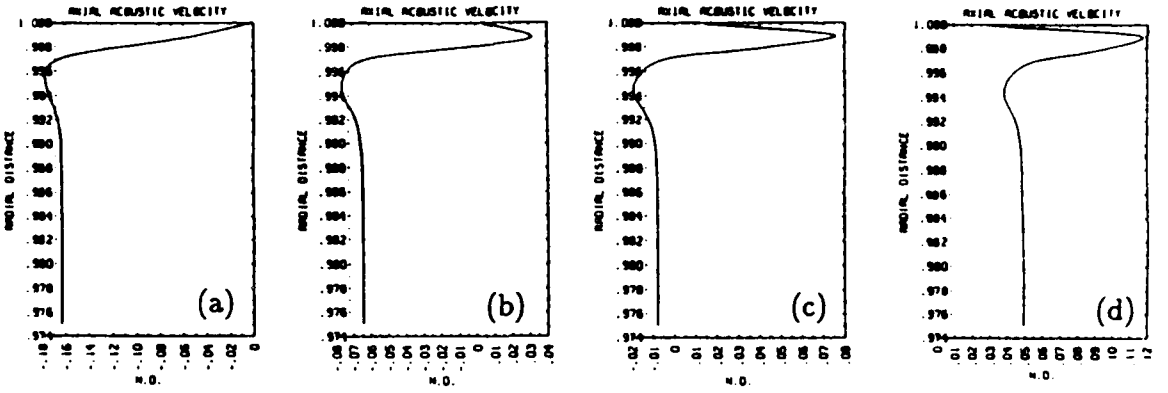

Fig. 9. Radial Distribution of Acoustic Velocity, No Mean Flow, f=1000 Hz, Z=0.378 m. (a) Time=2.01 ms. (b) Time=2.07 ms. (c) Time=2.09 ms. (d) Time=2.12 ms.

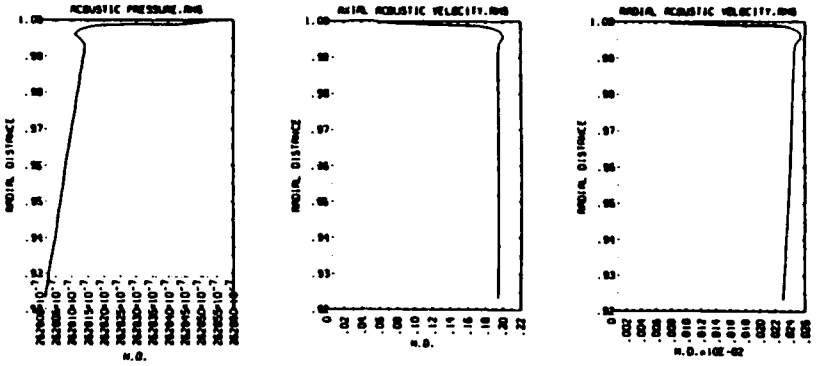

Fig. 10. Radial Distribution of Root Mean Squared Acoustic Pressure, Axial acoustic Velocity and Radial Acoustic Velocity, No Mean Flow, f=1000 Hz.

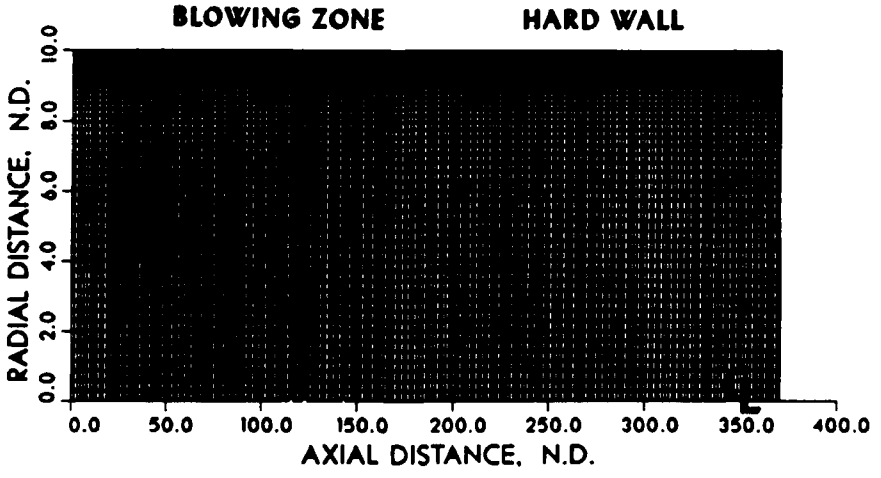

Fig. 11. Computational Grid Used for Flow Turning Study.

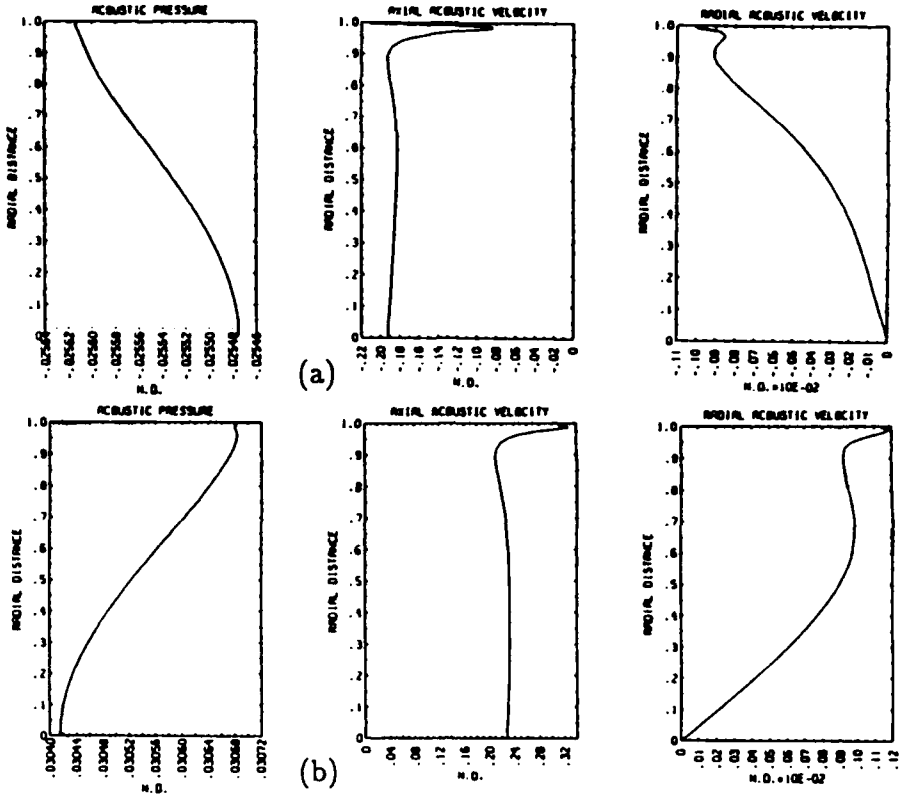

Fig. 12. Radial Distribution of Acoustic Pressure, Axial Acoustic Velocity and Radial Acoustic Velocity, Flow Turning Study, Z=1.004 m. (a) Time=4.24 ms. (b) Time=4.67 ms.

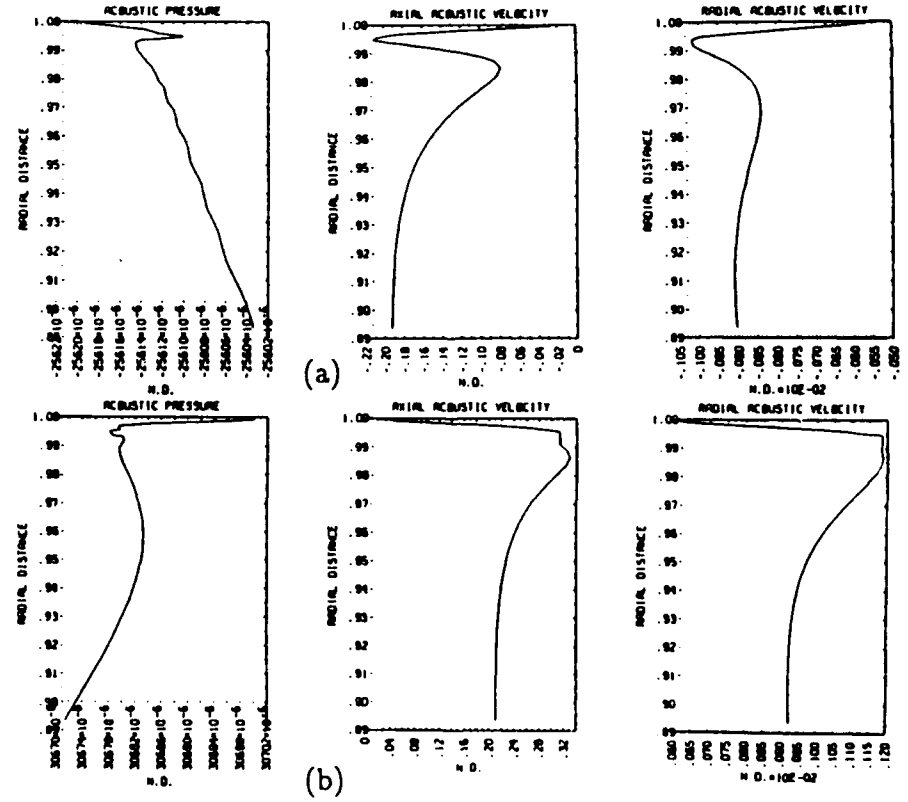

Fig. 13. Radial Distribution of Acoustic Pressure, Axial Acoustic Velocity and Radial Acoustic Velocity, Flow Turning Study, Z=1.004 m. R=0.9-1.0. (a) Time=4.24 ms. (b) Time=4.67 ms.

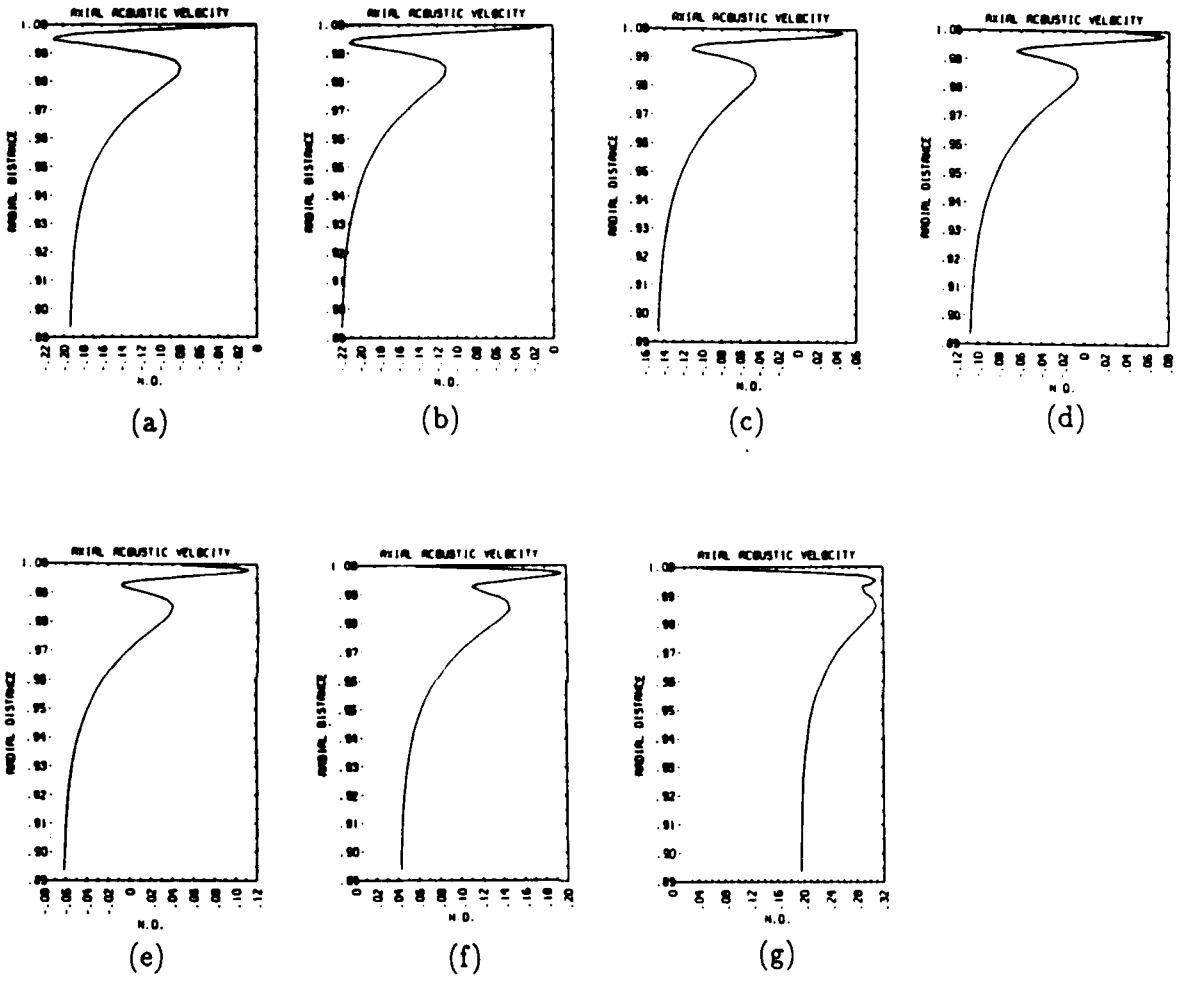

Fig. 14. Radial Distribution of Axial Acoustic Velocity, Flow Turning Study, Z=1.004 m. (a) Time=4.19 ms. (b) Time=4.29 ms. (c) Time=4.40 ms. (d) Time=4.43 ms. (e) Time=4.45 ms. (f) Time=4.53 ms. (g) Time=4.61 ms.

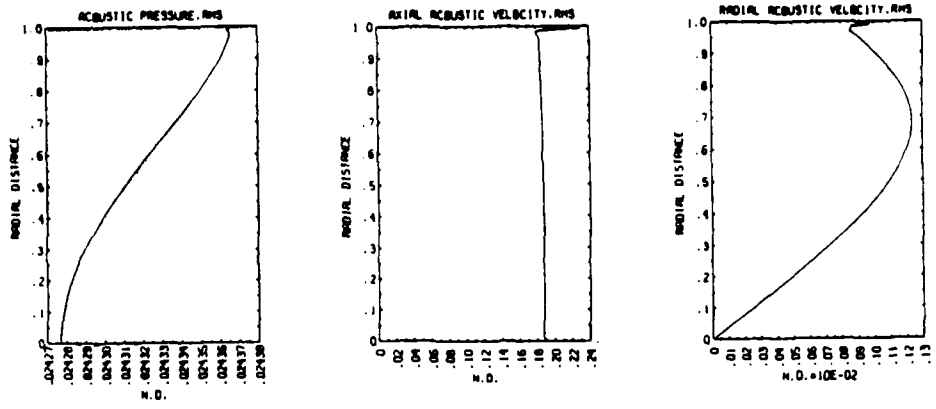

(a)

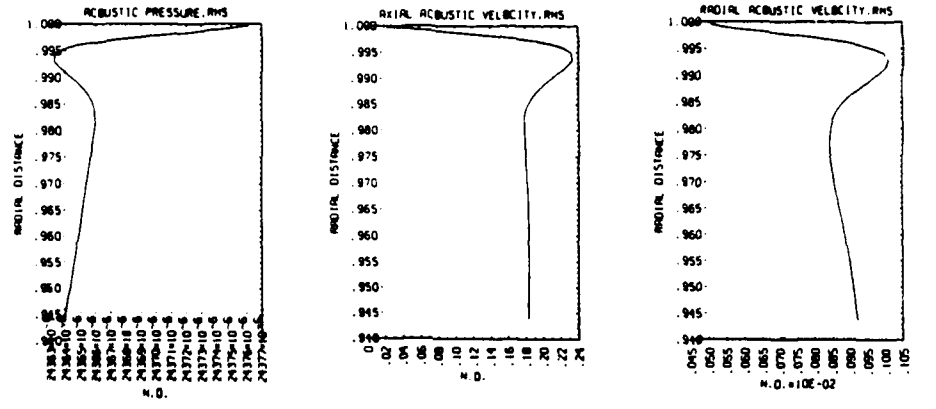

(b)

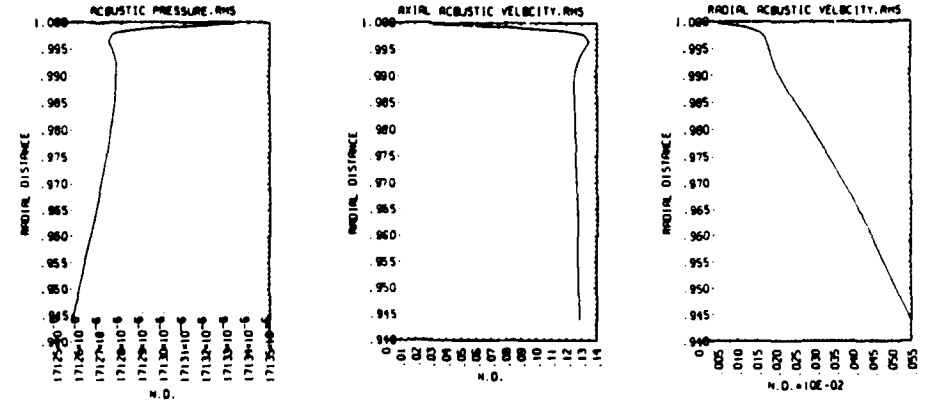

(c)

Fig. 15. Radial Distribution of Root Mean Squared Acoustic Pressure, Axial acoustic Velocity and Radial Acoustic Velocity, Flow Turning Study. (a) Z=0.377 m. R=0.0-1.0. (b) Z=0.377 m. R=0.945-1.0. (c) Z=1.279 m. R=0.945-1.0.

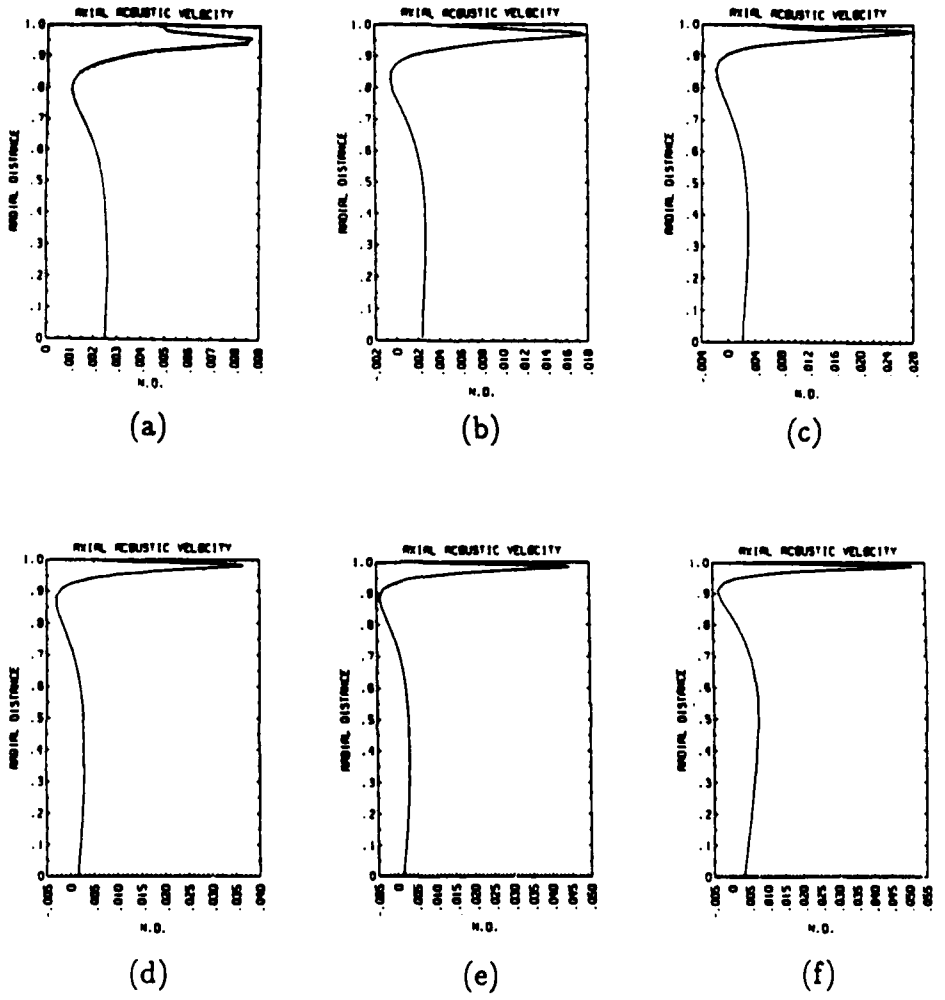

Fig. 16. Radial Distribution of Time Averaged Axial Acoustic Velocity, Flow Turning Study. (a) Z=0.257 m. (b) Z=0.429 m. (c) Z=0.600 m. (d) Z=0.772 m. (e) Z=0.994 m. (f) Z=1.115 m.

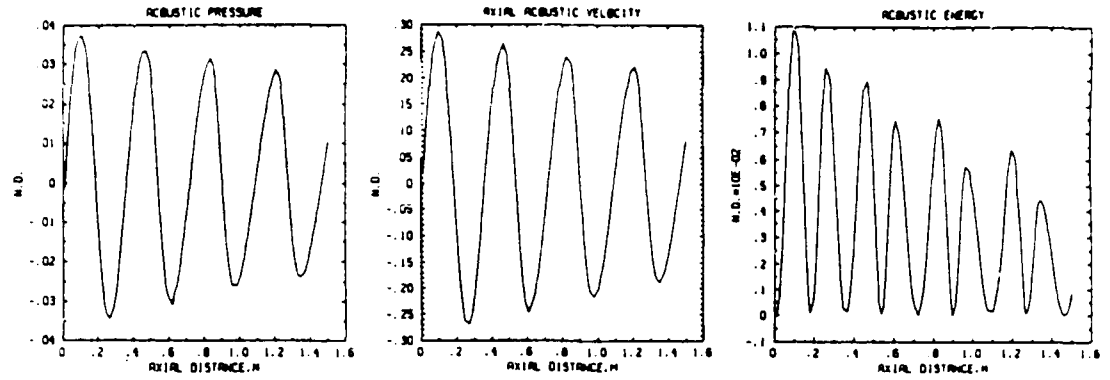

(a)

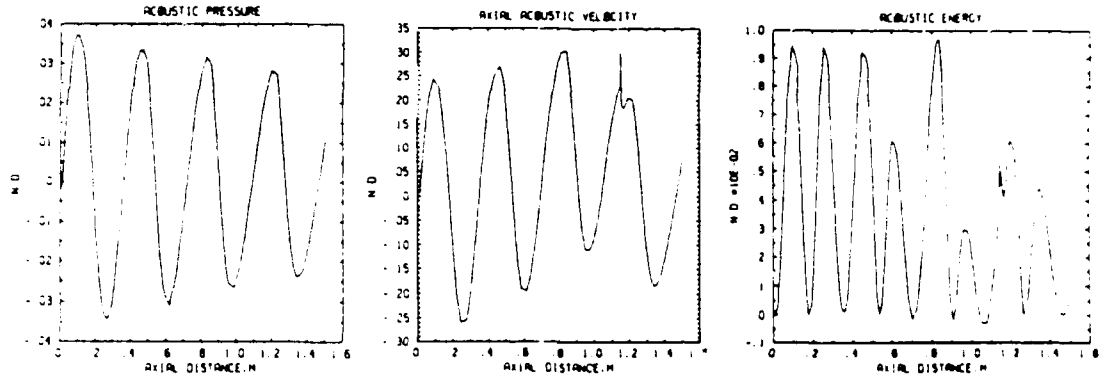

(b)

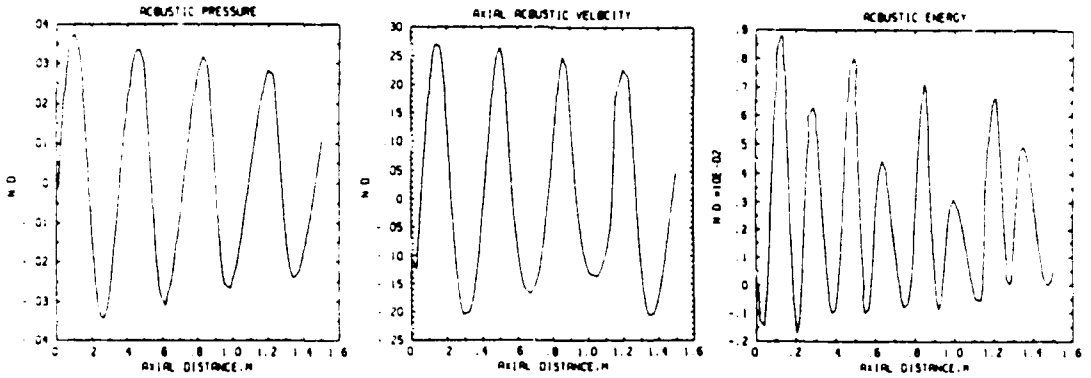

(c)

Fig. 17. Spatial Evolution of Acoustic Pressure, Axial Acoustic Velocity and Acoustic Energy, Flow Turning Study, Time=4.20 ms, (a) Centerline. (b) Distance to Wall=735 microns. (c) Distance to Wall=118 microns.

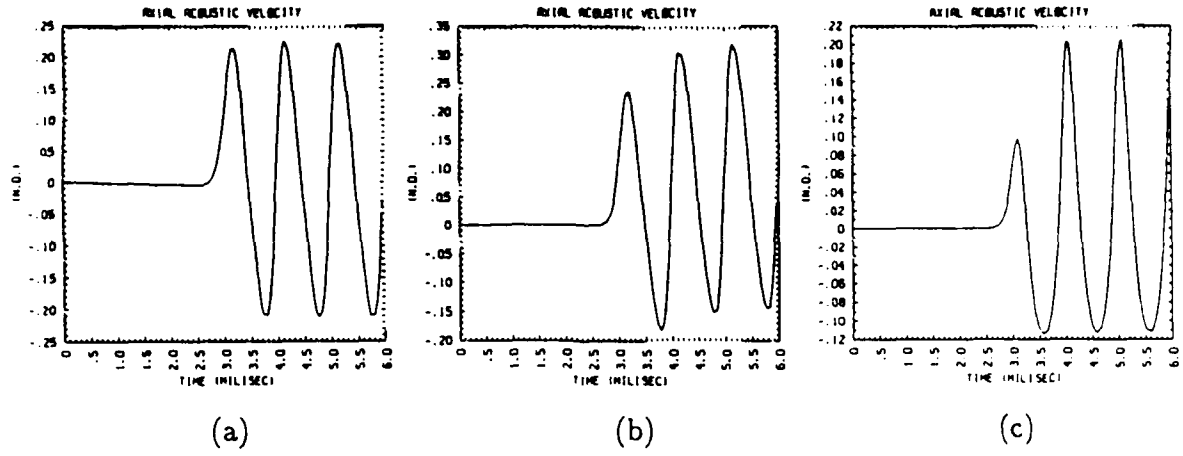

Fig. 18. Time Evolution of Axial Acoustic Velocity, Flow Turning Study, Z=1.059 m. (a) Centerline. (b) Distance to Wall=624 microns. (c) Distance to Wall=94 microns.

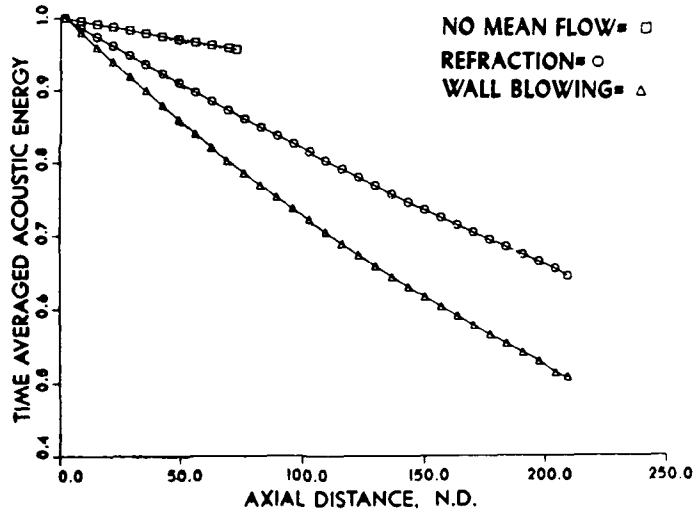

Fig. 19. Comparison of The Axial Distribution of Normalized Acoustic Energy for Refraction, No Mean Flow and Flow Turning Studies, f=1000 Hz.

ACKNOWLEDGMENTS

The authors wish to thank Dr Jayant S. Sabnis of SRA Inc. Hartford CT for his help with the MINT code. Partial funding for this research work was provided by AFOSR, program element 2308M1UF. Dr L. Caveny was program coordinator.

REFERENCES

1. Culick, F.E.C., "The Stability of One-Dimensional Motions in a Rocket Motor", *Combustion Science and Technology*, **Vol. 7** (1973), pp. 165-175.
2. Culick, F.E.C., "Nonlinear Behavior of Acoustic Waves in Combustion Chambers", Jet Propulsion Center, California Institute of Technology, Pasadena, California, April 1975. NASA-CR-149367.
3. Flandro, G.A., "Solid Propellant Acoustic Admittance Corrections", *Journal of Sound and Vibration*, **Vol. 36,** pp. 297-312 (1974).
4. Van Moorhem, W.K., "An Investigation of the Origin of the Flow Turning Effect in Combustion Instability", 17th JANNAF Combustion Meeting Langley, VA, September 1980, pgs. 301 – 320, Volume I (AD-A094 820).
5. Chung, T.J. and Hackett, R.M., "A New Approach to Combustion Instability Analysis for Solid Propellant Rocket Motors", 19th JANNAF Combustion Meeting, NASA Goddard Space Flight Center, Greenbelt, Maryland, 4-7 pages 219 – 234, October 1982. (AD-A126 986).
6. Culick, F.E.C. and Magiawala, K., "Measurements of Energy Losses Associated with Interactions Between Acoustic Waves and a Steady Flow Field", 78-6, November 1977. AFPRL-TR-6 (AD-A054 532)
7. Hersh, A.S. and Walker, B., "Experimental Investigation of Rocket Motor Flow Turning Loses", AIAA paper 83-1267, presented at the AIAA/SAE/ASME 19th Joint Propulsion Conference, Seattle, Washington, June 27-29, 1983.
8. Hersh, A.S. and Walker, B., "Experimental Investigation of Rocket Motor Flow Turning Acoustic Losses", AFRPL TR-84-009, May 1984. (AD-A144 168)
9. Richardson, E.G. and Tyler, E., "The Transverse Velocity Gradient Near the Mouths of Pipes in Which an Alternating or Continuous Flow of Air is established", *The Proceedings of the Physical Society*, **Vol. 42,** Part 1, No. 231, 1929, pp. 1-15.
10. Uchida, S., "The Pulsating Viscous Flow Superposed on the Steady Laminar Motion of Incompressible Fluid in a Circular Pipe", *ZAMP*, **Vol. 7,** 1956, pp. 403 – 422.
11. Romie, F.E., "Heat Transfer to Fluids Flowing with Velocity Pulsations in a Pipe", Ph.D. Dissertation, UCLA, 1956.

12. Barnett, D.O., "An Analytical Investigation of Heat Transfer in Pulsating Turbulent Flow in a Tube", Ph.D. Dissertation, Auburn University, 1970.

13. Feiler, C.E., "Experimental Heat-Transfer and Boundary-Layer Behavior with 100-CPS Flow Oscillations", NASA TN D-2521, December 1964. N65-12079.

14. Bogdanoff, D.W., "A Study of the Mechanisms of Heat Transfer in Oscillating Flow", TR 483-f, Department of Aerospace and Mechanical Sciences, Princeton University, 1967. (AD-664 248)

15. Clamen, M. and Minton, P., "An Experimental Investigation of Flow in an Oscillating Pipe", *Journal of Fluid Mechanics*, **Vol. 81,** pp. 421 – 431, 1977.

16. Richardson, P.D., "Effects of Sound and Vibrations on Heat Transfer", *Applied Mechanics Reviews*, **Vol. 20,** pp. 201 – 217, 1967.

17. Mickelsen, W.R. and Laurence, J.C., "Measurement and Analysis of Turbulent Flow Containing Periodic Flow Fluctuations", NACA RM E53F19, August 1953. (AD-015 616)

18. Richardson, E.G., "The Amplitude of Sound Waves in Resonators", *Proceedings of the Physical Society*, **Vol, 40,** No. 206, 1928, pp. 206 – 220.

19. Mohajery, M., "An Experimental Study of the Structure of the Pulsating Turbulent Flow of Air in a Circular Pipe", Ph.D. Dissertation, Clarkson College of Technology, 1973.

20. Sexl, T., "Annular Effect in Resonators Observed by E.G. Richardson", *Zeitschrift fur Physik*, **Vol. 61,** 1930, pp. 349-362.

21. Barnett, D., "The Effect of Pressure Pulsations and Vibrations Fully Developed Pipe Flow", AEDC-TR-80-31 Report, Arnold Engineering Development Center, August, 1981. (AD-A 103 330)

22. Richardson, E.G., *Dynamics of Real Fluids*, 2nd ed. Arnold, London, 1961.

23. Baum, J.D., and Levine, J.N. "Numerical Study of Acoustic Refraction Phenomenon", AIAA-84-2255, presented at the AIAA/NASA 9th Aeroacoustics Conference, Williamsburg, VA, Oct 15-17, 1984.

24. Pridmore-Brown, D.C., "Sound Propagated in Fluid Flowing through an Attenuating Duct", Journal of Fluid Mechnics, Vol. 4, 1958, p. 393 – 406.

25. Hersh, A.S. and Catton, I., "Effect of Shear Flow on Sound Propagation in Rectangular Ducts", *The Journal of the Acoustical Society of America*, **Vol. 50,** No. 3, p 922 – 1003, 1971.

26. Munger, P. and Gladwell, G. M. L., "Acoustic Wave Propagation in a Sheared Flow Contained in a Duct", *Journal of Sound and Vibration*, **Vol. 9,** 1969, p. 28 – 48.

27. Munger, P. and Plumblee, H.E., "Propagation and Attenuation of Sound in an Annular Duct Containing an Sheared Flow", Presented at the NASA Basic Noise Research Conference, 14-15 July, 1980.

28. Hersh, A.S., Private Communications.

29. Briley, W.R. and McDonald, H., "Solution of the Multidimensional Compressible Navier-Stokes Equations by a Generalized Implicit Method", *Journal of Computational Physics,* **Vol. 24,** pp. 372-397, 1977.

30. Briley, W.R. and McDonald H., "On the Structure and Use of Linearized Block Implicit Schemes", *Journal of Computational Physics,* **Vol. 34,** pp. 54-73, 1980.

31. Launder, B.E. and Spalding, D.B., "Lectures in Mathematical Models of Turbulence", Academic Press, 1972.

32. Jones, W.P., and Launder, B.E. "The Prediction of Laminarization with a Two-Equation Model of Turbulence", *Int. J. of Heat and Mass Transfer,* **Vol. 15,** pp. 301-314, 1972.

33. Sabnis, J.S., Gibeling, H.J. and H. McDonald "Calculation of Solid Propellant Rocket Motor Internal Flow Field Using an Implicit Navier-Stokes Procedure", AIAA paper 85-1625, presented at the AIAA 18th Fluid and Plasma Dynamics Conference, Cincinnati, Ohio, July 16-18, 1985.

34. Simpson, R.L., "Characteristics of Turbulent Boundary Layers at Low Reynolds Numbers with and without Transpiration", *Journal of Fluid Mechanics,* **Vol. 42,** Part 4, 1970, pp. 769-802.

END

11-86

DTIC